國立臺灣大學工學院應用力學研究所

碩士論文

Institute of Applied Mechanics

College of Engineering

National Taiwan University

Master's Thesis

利用新的數學模型分析老化與高血壓對腦血流自動調節的影響

Analysing the effects of ageing and hypertension on dynamic cerebral autoregulation using a new mathematical model

黃國翔

Guo-Xiang Huang

指導教授：潘斯文 博士

Advisor : Stephen Payne, Ph.D.

中華民國 113年 7月

July, 2024

doi:10.6342/NTU202403077

致謝

在台大這兩年是我學習生涯中最充實的時光之一。首先，我要感謝我的老師潘斯文教授，在研究以及論文方面給予我的指導和幫助，即使研究方面遇到困難您也會給我方向好讓我培養解決問題的能力。同時這兩年您也給了我很多時間充實自己，讓我能夠去探索自己對於未來的職涯規劃。

再來，我要感謝在研究生活中常常一起說笑的好夥伴宇真，常常跟我從事一些好玩的活動；感謝我研究中的得力夥伴韋皓，教會了我如何快速上手程式語言以及在研究上幫了我許多大忙；還有必修課的好夥伴人鳳，在課程方面常常提醒我什麼時候要交作業以及常常給我一些課堂筆記。

此外，我要感謝實驗室助理弘奇，你在課務上的幫忙和支持讓我們能專心於研究工作，還有文逢口委在我的論文修改上給出了許多寶貴的建議，還有感謝元中學長在修課及研究方面給予了我許多寶貴的建議和指導然後也是我說笑的好夥伴。

同時，我要感謝學弟妹們集龍、珈朵以及杰成，你們的加入讓實驗室的氣氛變得更加活躍和充滿活力，希望你們能夠將實驗室的氣氛繼續維持好傳承下去。

最後，我特別感謝我的女朋友邵恩，在這條求學的路上，你一直陪伴著我，給予我無盡的支持和鼓勵。還有我的家人們，感謝你們一直以來的支持和鼓勵，這些都成為我前進的動力。

當然，也要感謝其他實驗室的夥伴以及學弟妹們，還有大學同學以及實習朋友們的陪伴。有你們的幫助，這篇論文得以順利完成。

黃國翔 2024.07

doi:10.6342/NTU202403077

Acknowledgements

The past two years at NTU have been some of the most fulfilling of my academic career. Firstly, I must express my gratitude to my teacher Stephen for his guidance and assistance in research and thesis writing. Despite challenges, you provided direction and nurtured my problem-solving skills, while also allowing me time to enrich myself and explore future career plans.

Additionally, I thank my cheerful friend Jimmy, who often engaged in fun activities with me; my reliable study partner Howard, who taught me how to quickly pick up programming languages and greatly assisted my research; and Lucia, my dependable classmate who often reminded me about assignment deadlines and generously shared her notes.

Moreover, my appreciation extends to lab assistant Oran, whose support in academic matters allowed us to focus on our research, and Mike, a member of the thesis review committee, provided many valuable suggestions for revisions to my thesis, and senior Paul, who provided valuable advice on coursework and research and was also a great companion for laughs.

I am also grateful to my juniors Tomy, Dory, and Francisco, whose presence added more vitality to our lab atmosphere. I hope you continue to foster this lively

doi:10.6342/NTU202403077

environment.

Lastly, special thanks to my girlfriend Ivy, who has been by my side throughout this academic journey, providing endless support and encouragement, and to my family, whose encouragement has been a driving force.

Of course, thanks to all other lab mates, juniors, university classmates, and internship friends whose companionship helped me successfully complete this thesis.

Thank you all!

doi:10.6342/NTU202403077

中文摘要

腦血流自動調節的干擾可能會嚴重影響大腦健康，並可能導致各種疾病，如老化和高血壓。因此，有了病人的血壓和血流量等臨床數據，我們可以利用數學模型來觀察自動調節曲線，並預測疾病的潛在發生。

然而，一氧化氮模型參數過多，使臨床分析和預測變得複雜。出於需要有效處理腦血流自動調節涉及的不同時間尺度的必要，提出了新的數學模型的需求。在擬合參數之後，建立了新的腦血流自動調節曲線，顯著減少了參數的數量。

此外，新的數學模型引入了進行性血管活性功能障礙公式，以觀察不同年齡組的腦血流自動調節。 我們的結果顯示，在新的數學模型中，我們調整了11個參數，顯著減少了總參數數量，同時滿足了自動調節曲線分佈的預期。

在穩態分析中，引入進行性血管活性功能障礙公式後，不同年齡組的自動調節曲線分佈符合預期，使得能夠對不同年齡組的高血壓患者進行可測試的預測。在動態狀態分析中，趨勢保持一致，顯示隨著年齡增長，血管半徑和血流量下降，表明新模型能有效預測老化和高血壓患者的病情。

關鍵字：腦血流; 腦血流自動調節; 柯西應力張量; 老化; 高血壓; 進行性血管活性功能障礙

doi:10.6342/NTU202403077

Abstract

Disruptions in cerebral blood flow autoregulation can significantly impact brain health, potentially leading to various diseases such as ageing and hypertension. Therefore, with clinical data on a patient's blood pressure and blood flow, we can use mathematical models to observe the autoregulation curve and predict the potential onset of diseases. However, the nitro-oxide model had too many parameters, complicating clinical analysis and predictions. The need for a new mathematical model arises from the necessity to effectively address different time scales involved in cerebral blood flow autoregulation. After fitting the parameters, a new cerebral blood flow autoregulation curve is established, significantly reducing the number of parameters.

In addition, the new mathematical model introduces a progressive vasoactive dysfunction formula to observe cerebral blood flow autoregulation across different age groups. Our results show that in the new mathematical model, we adjusted 11 parameters, reducing the total number significantly while meeting expectations for the autoregulation curve's distribution.

In steady state analysis, after incorporating the progressive vasoactive dysfunction formula, the distribution of autoregulation curves across different age groups met expectations, allowing testable predictions for hypertensive patients across age groups.

doi:10.6342/NTU202403077

In dynamic state analysis, the trends remained consistent, showing a decline in blood vessel radius and blood flow with ageing, indicating the new model can effectively be used to predict conditions in ageing and hypertension patients.

Keywords: Cerebral blood flow; Cerebral blood flow autoregulation; Cauchy stress tensor; Ageing; Hypertension; Progressive vasoactive dysfunction;

doi:10.6342/NTU202403077

Contents

doi:10.6342/NTU202403077

doi:10.6342/NTU202403077

doi:10.6342/NTU202403077

doi:10.6342/NTU202403077

List of Figures

doi:10.6342/NTU202403077

doi:10.6342/NTU202403077

doi:10.6342/NTU202403077

List of Tables

doi:10.6342/NTU202403077

Chapter 1

Introduction

The brain, serving as the paramount central system for the human body, plays a crucial role in controlling and coordinating bodily functions. A vital component of brain functionality is the cerebral vasculature system, primarily responsible for regulating the pressure and volume of cerebral blood flow (CBF) to maintain homeostasis within the brain [1]. However, sudden alterations in the cerebral vascular system can lead to significant disruptions in the stability of CBF, potentially resulting in severe intracranial diseases, such as Alzheimer's disease and stroke that can be caused by ageing and hypertension. Fortunately, there is a significant interest in brain health, leading to numerous studies in the past that have focused on simulating the dynamics of CBF. Upon establishing models for the brain's vasculature, blood flow, and pressure, these studies have laid the groundwork for dynamic monitoring models based on the mechanisms of CBF autoregulation [2]. These models have been validated with clinical data on various cerebral blood flow-related diseases to ensure accuracy and thus facilitate effective clinical predictions [3]. However, previous models were primarily based on physiological and chemical properties, which

doi:10.6342/NTU202403077

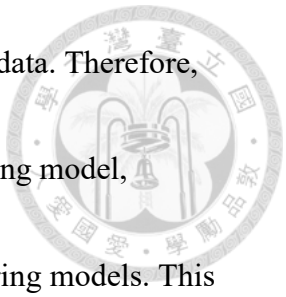

significantly increased the complexity and volume of the simulation data. Therefore, this research proposes a novel mechanical model to replace the existing model, thereby simplifying its complexity and establishing dynamic monitoring models. This model uniquely considers different time scales and explicitly incorporates the effects of ageing and hypertension, which are not adequately addressed in current models. This chapter will delve into cerebral blood flow, diseases related to cerebral blood flow, and clinical diagnostic methods.

1.1 Cerebral Blood Flow

To better understand the dynamics of blood flow, it's crucial to first comprehend the basic anatomy of how blood circulates through the body, particularly to the brain. Blood is pumped from the heart through arteries that distribute it to all body parts, including the brain. Specifically, cerebral blood flow (CBF) targets the brain’s regions, delivering essential nutrients and metabolic substances vital for brain functions. However, disruptions in CBF can precipitate severe cerebral diseases. Future sections will further outline the operational mechanisms of cerebral circulation and the critical role of autoregulation. Additionally, a detailed

doi:10.6342/NTU202403077

description of the cerebral vasculature will be provided to enhance understanding of its influence on overall brain health.

1.1.1 Basic Function of Blood Flow

Blood primarily consists of erythrocytes (red blood cells), leukocytes (white blood cells), platelets, and plasma [4]. Plasma constitutes 50%-60% of blood and is considered to closely resemble a Newtonian fluid in its analysis.

It serves as the liquid matrix that carries not only nutrients and waste products but also the blood cells themselves. Red blood cells (RBCs), which make up most of the cellular components, are crucial for transporting oxygen from the lungs to the body's tissues and bringing carbon dioxide back for exhalation. White blood cells (WBCs), though fewer, play essential roles in the immune response, protecting the body against infection and disease. However, under certain pathological conditions, the viscosity of blood can increase, particularly due to changes in RBC concentration and WBC activity.

doi:10.6342/NTU202403077

Thus, the assumption of blood behaving as a Newtonian fluid becomes significantly less accurate with decreasing vessel diameter under high strain rates. Therefore, given the limitations of the Newtonian fluid assumption under high strain rates and smaller vessel diameters, we propose employing the most common non-Newtonian relationships (Figure 1.1). This approach aims to achieve a more accurate fit between blood's shear stress and strain rate, thereby significantly enhancing the realism and precision of our models, especially in scenarios where pathological conditions alter blood's typical behaviour.

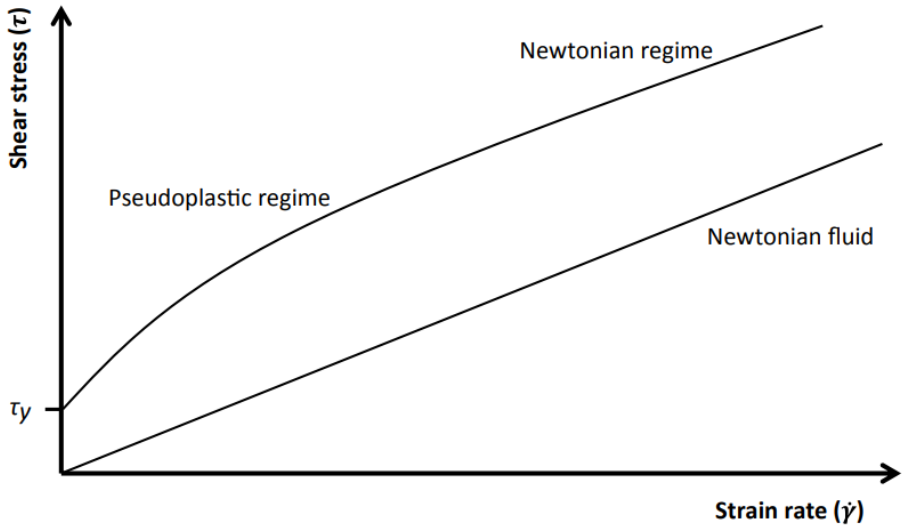

Figure 1.1 Characteristic flow behaviour for blood. (Figure reproduced from [39]).

doi:10.6342/NTU202403077

1.1.2 Cerebral Autoregulation

An important factor related to cerebral blood flow (CBF) is its autoregulation, which utilizes the relationship between blood pressure and blood flow to maintain cerebral homeostasis (Figure 1.2) [3]. This regulatory mechanism is crucial as it ensures that blood pressure and flow achieve a balance within normal ranges, thus preventing excessive blood flow that could be caused by high blood pressure.

Static cerebral autoregulation (sCA) refers to the brain's ability to maintain constant CBF despite slow changes in arterial blood pressure, serving as a benchmark for assessing overall brain health and functioning as a baseline condition for more detailed studies. On the other hand, dynamic cerebral autoregulation (dCA) addresses how quickly the cerebral vessels can react to rapid fluctuations in blood pressure. Quantifying dCA involves measuring the time-dependent response of CBF to these changes, which is critical for understanding the brain's ability to protect itself during sudden blood pressure alterations such as those occurring during physical activities or acute medical events.

doi:10.6342/NTU202403077

Both sCA and dCA are integral to maintaining cerebral homeostasis, but they operate on different timescales and are relevant to different physiological and pathological scenarios. Understanding both is essential for a comprehensive assessment of cerebral autoregulation capabilities [6].

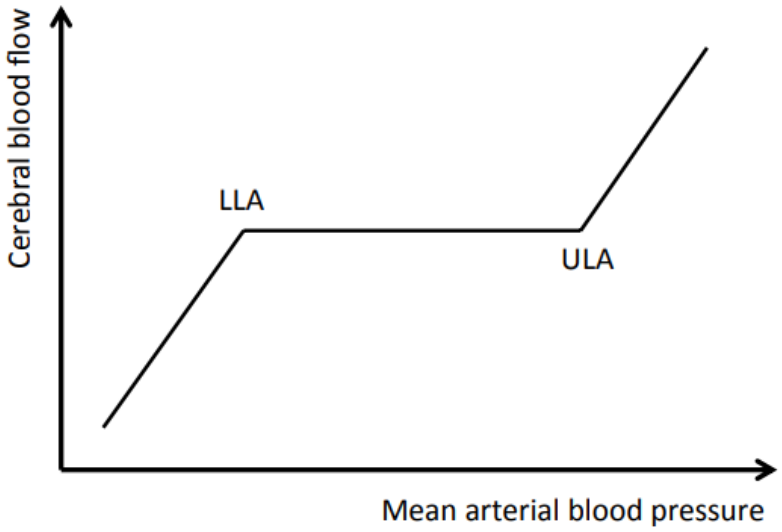

Figure 1.2 Classical view of cerebral autoregulation. (Figure reproduced from [39]).

1.2 Diseases Related to CBF

Diseases that affect static and dynamic cerebral autoregulation (sCA/dCA) can compromise the brain's protection mechanisms. Impairments such as a delayed response in the autoregulatory curve or a sudden decrease in cerebral blood flow (CBF)

doi:10.6342/NTU202403077

can therefore lead to a variety of severe brain-related diseases. Given the brain's central role in human function, these damages are often irreversible and severe. This section will introduce hypertension as a classic disease associated with dysfunction of cerebral blood flow autoregulation and discuss how ageing, a natural physiological process, also impacts this autoregulation.

1.2.1 Ageing

Ageing primarily affects the elderly, causing many impacts such as changes in cerebral circulation, perfusion, cerebrovascular reactivity, autoregulation, and neurovascular coupling. This leads to reduced microvascular density, decreased blood flow, and increased permeability. Based on different time scales, perfusion reduction can be categorized into gradual decreases throughout the adult lifespan and e‑mbolism, a medical condition that can occur suddenly at any time, is not solely a consequence of ageing. However, the risk of developing an embolism increases with age due to changes in blood composition and vessel integrity, making it a significant concern for older adults. It has been well established that CBF negatively correlates with age (Figure 1.3), suggesting that the mechanisms of ageing can be controlled by

doi:10.6342/NTU202403077

monitoring the behaviour of cerebral blood flow.

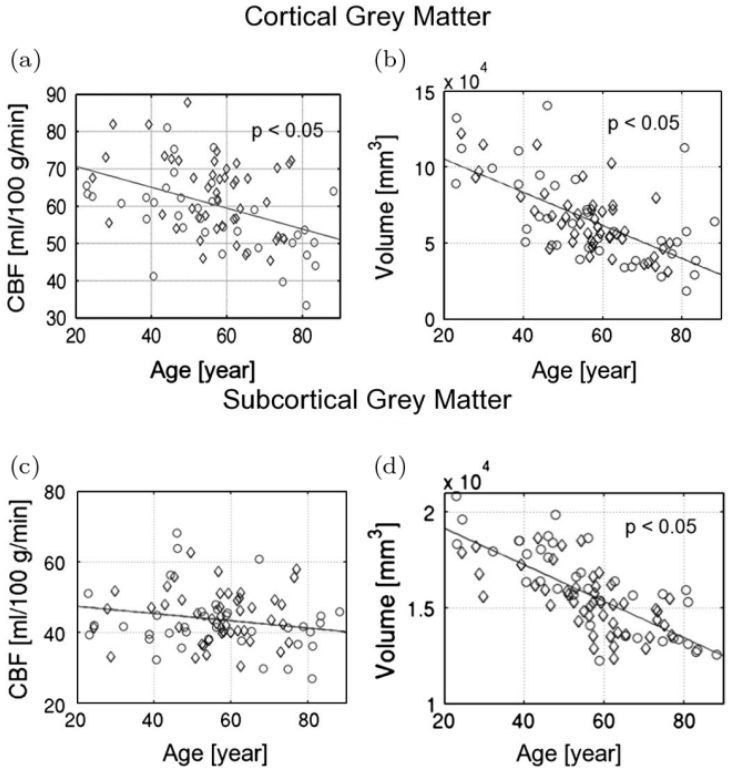

Figure 1.3 Variation in cerebrovascular reactivity and cerebral blood flow with age. (Figure reproduced from [7]).

Ageing leads to a reduction in microvessel density, decreased blood flow, and increased permeability (Figure 1.4), with these changes being particularly pronounced in the elderly population and there is an increasing number of elderly people over 65 years old in Taiwan (Figure 1.5). With the increase in ageing-related conditions, detecting markers of vascular ageing has become crucial, and aim to utilize the

doi:10.6342/NTU202403077

transient relationship between cerebral artery blood pressure and cerebral blood flow (CBF) to assess vascular ageing effects.

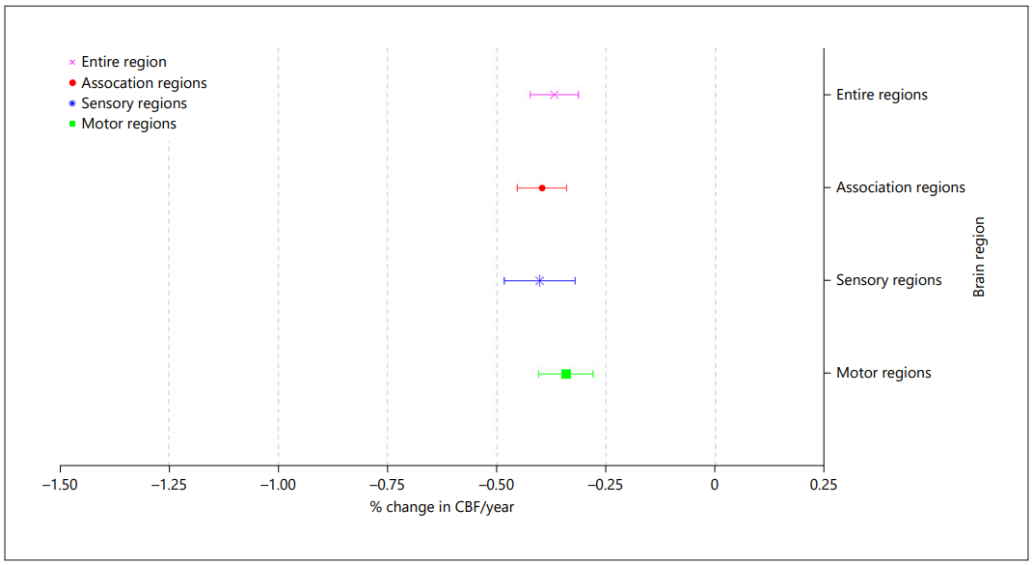

Figure 1.4 Weighted summary mean and 95% CI values of CBF with healthy ageing. (Figure reproduced from [8]).

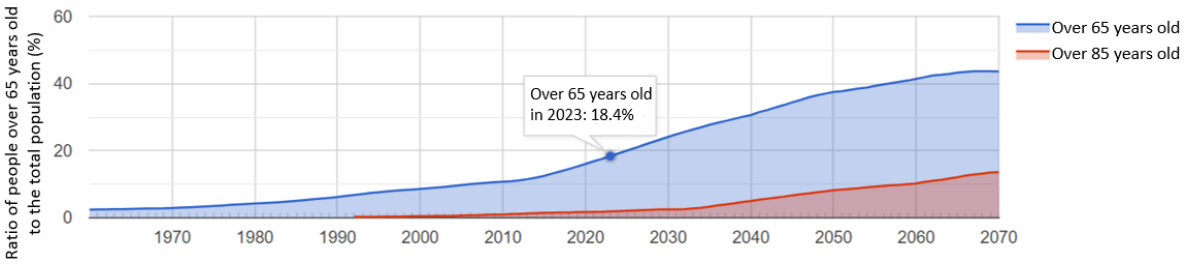

Figure 1.5 Taiwan's population trend over 65 years old. (Figure reproduced from [9]).

doi:10.6342/NTU202403077

1.2.2 Hypertension

Hypertension is defined as a systolic pressure of ≥140 mmHg and a diastolic pressure of ≥90 mmHg [10]. One of the organs that hypertension most severely damages is the brain, leading to severe diseases such as stroke and Alzheimer's disease. The cause is related to a reduced cross-sectional area of the vessels, resulting in increased resistance. Additionally, the aortic walls stiffen with time. Arteriosclerosis of the major extracranial and intracranial arteries results from alterations in autoregulation, neurovascular coupling, and blood-brain barrier permeability. This could be the result of shifting wall shear stress, causing microhaemorrhages and extensive haemorrhages. (Figure 1.6), in Taiwan, it is estimated that approximately 5.29 million individuals suffer from hypertension [11], with the prevalence increasing as age progresses.

doi:10.6342/NTU202403077

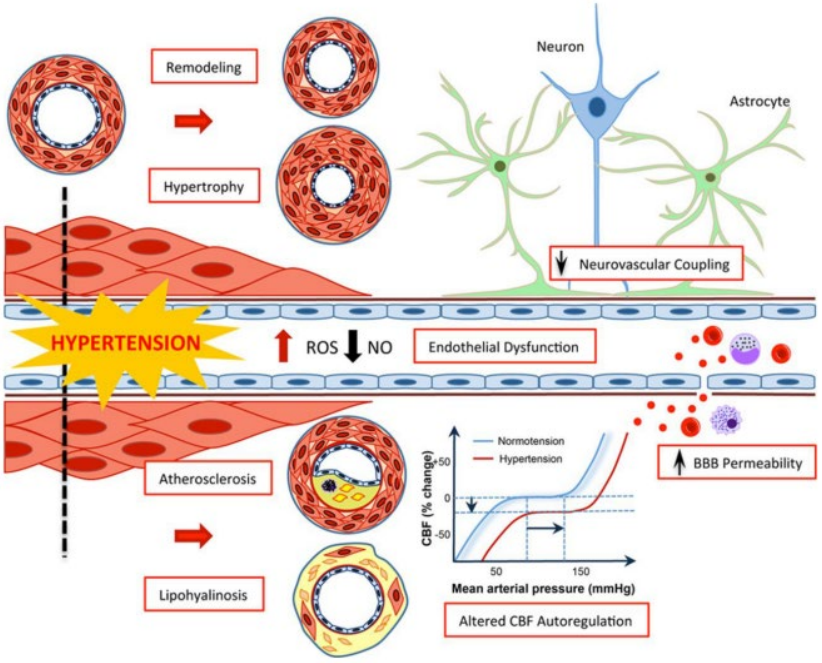

Figure 1.6 Schematic of effects of hypertension on cerebral blood vessels. (Figure reproduced from [12]).

Although the exact causes of hypertension remain unknown, the impact of ageing on health is well-documented. It is evident that utilizing the mechanism of cerebral blood flow autoregulation can both prevent and assess cerebrovascular diseases, addressing these critical factors. For example, the impact of ageing on brain health can be assessed by monitoring reductions in cerebral blood flow (CBF). In the case of hypertension, it can be evaluated by observing shifts in the cerebral autoregulation curve, specifically whether it moves leftward or downward, indicating changes in the brain's ability to regulate blood flow under varying levels of blood pressure.

doi:10.6342/NTU202403077

1.3 Clinical Measurements

Cerebral blood flow autoregulation is crucial for brain health, and changes in this process can lead to various diseases. Clinically, we measure changes in autoregulation trends by monitoring patients' blood flow rate and blood pressure. This chapter primarily discusses three common clinical prediction methods: Positron Emission Tomography (PET), Magnetic Resonance Imaging (MRI), 4D Flow MRI and Transcranial Doppler (TCD).

1.3.1 Computed Tomography (CT)

Computed Tomography (CT), which was developed in the early 1970s, is a sophisticated imaging method that creates comprehensive cross-sectional images of the body by using X-rays in conjunction with complex computational techniques. It creates high-resolution, three-dimensional images by capturing several X-ray pictures from various angles. These images are essential for identifying anomalies in the abdomen, chest, brain, and other areas of the body.

doi:10.6342/NTU202403077

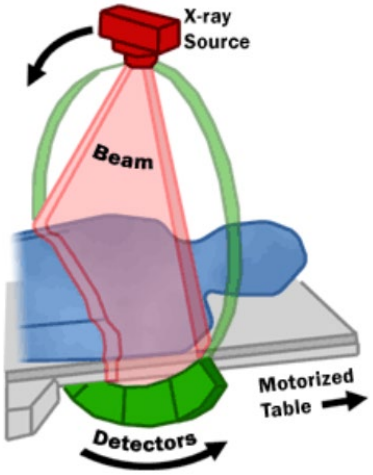

Figure 1.7 Drawing of CT fan beam (left) and patient in a CT imaging system (Figure reproduced from [44]).

1.3.2 Positron Emission Tomography (PET)

Positron Emission Tomography (PET) is a sophisticated imaging method that employs radiopharmaceuticals. This technique utilizes a radiotracer known for emitting positrons, captured by detectors encircling the patient. PET scans are particularly beneficial for revealing blood flow patterns and can be integrated with CT or MRI scans to enhance diagnostic precision. Commonly, PET is utilized for diagnosing and tracking cancer, evaluating brain functions, and investigating various medical conditions. The process of PET imaging is depicted in a schematic in Figure 1.8.

doi:10.6342/NTU202403077

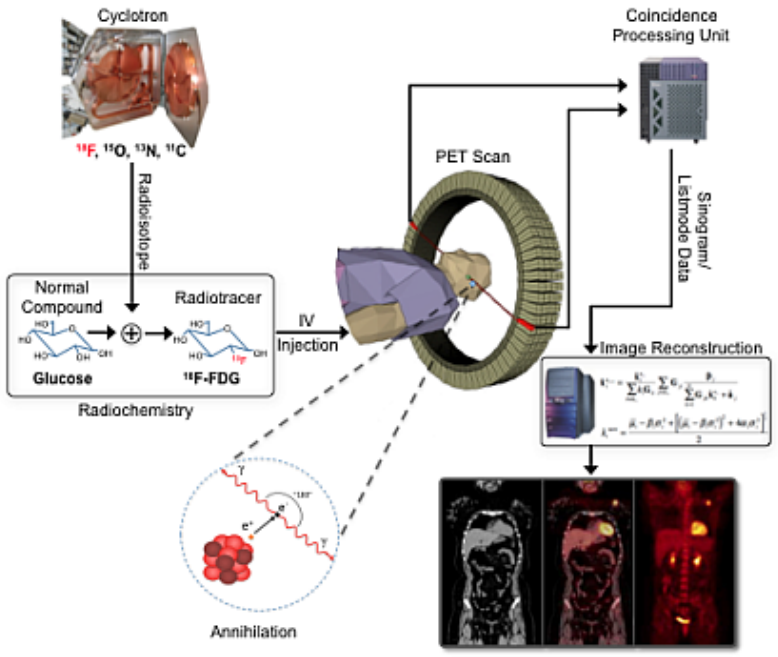

Figure 1.8 The process of PET. (Figure reproduced from [13]).

1.3.3 Magnetic Resonance Imaging (MRI)

Magnetic Resonance Imaging (MRI) is a non-invasive technique that produces accurate images of the body's internal structures by utilising strong magnetic fields and radio waves. The MRI scanner, typically a large cylindrical apparatus, envelops the patient in a powerful magnetic field and emits radio wave pulses to create detailed images (Figure 1.9). These scanners come in a range of designs, from narrow tunnels to more open configurations.

doi:10.6342/NTU202403077

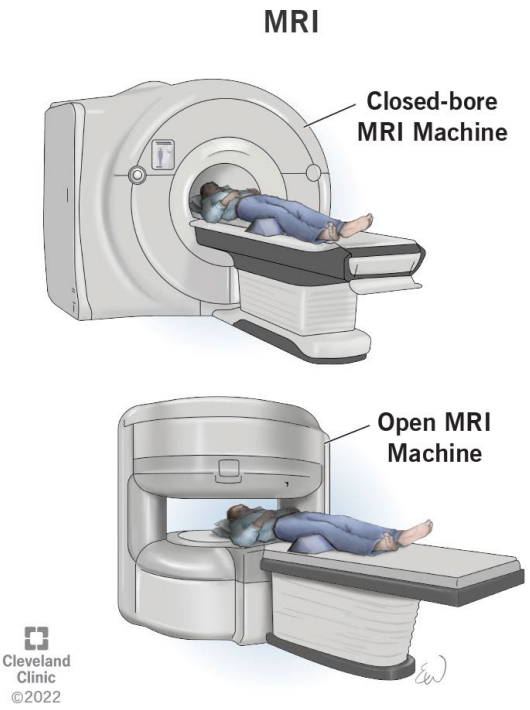

Figure 1.9 The two types of MRI. (Figure reproduced from [14]).

MRI is preferred over CT for examining soft tissues due to its superior ability to differentiate between various soft tissues and identify abnormalities. MRI, particularly advanced forms like 4D flow MRI, is crucial in studying cerebral haemodynamics and understanding autoregulation in clinical settings.

doi:10.6342/NTU202403077

1.3.4 4D flow MRI

4D Flow MRI is an advanced magnetic resonance imaging technique that utilizes time-resolved MRI to capture three-dimensional visualizations of blood flow dynamics (Figure 1.10). Compared to traditional MRI, it can capture comprehensive data on blood flow velocity and direction, enabling clinicians to observe and analyze patterns and changes in blood flow more accurately.

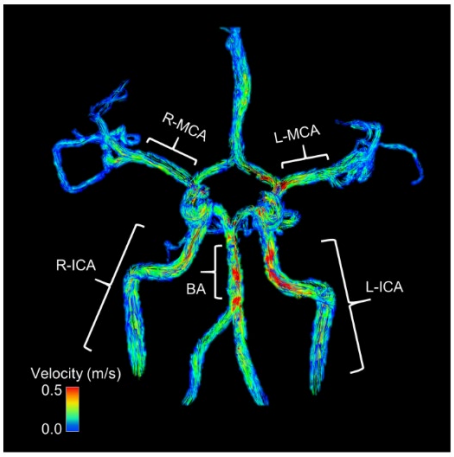

Figure 1.10 This 4D flow MRI image displays blood flow in warmer colors, averaging flow and vessel area along key cerebral arteries to calculate global flow. (Figure reproduced from [15]).

doi:10.6342/NTU202403077

Unlike traditional MRI, which only provides static images of tissues, 4D Flow MRI continuously tracks changes in blood flow, offering additional physical properties. This makes it exceptionally effective in studying cerebrovascular reactivity and autoregulation. 4D Flow MRI can assess whether these processes are affected by factors such as ageing or disease. This technique is not only used for diagnosing brain disorders, such as cerebrovascular anomalies or cerebral blood flow obstructions, but also helps physicians understand the progression of diseases and their specific impacts on cerebral blood flow, thereby guiding more precise treatment plans.

1.3.5 Transcranial Doppler (TCD)

Transcranial Doppler (TCD) is a non-invasive ultrasound technique used to measure blood flow velocity within intracranial vessels. This technology involves placing a probe at specific points on the scalp to monitor haemodynamic changes in real-time, making it a crucial tool for assessing cerebral blood flow and cerebral autoregulation. TCD is extensively used to study cerebrovascular diseases such as stroke, aneurysms, and cerebral vasospasm, and is primarily employed to monitor dCA.

doi:10.6342/NTU202403077

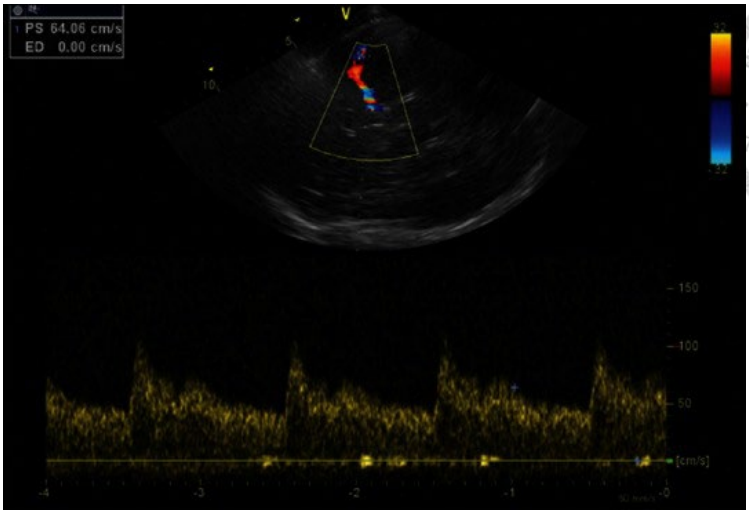

Figure 1.11 Transcranial Doppler spectral Doppler study of intracranial middle cerebral artery. (Figure reproduced from [45]).

Using the aforementioned advanced medical imaging technologies, we can obtain clinical data on patients' cerebral blood flow autoregulation. These data can be used in conjunction with developed mathematical models for validation, thereby facilitating effective prevention and prediction of cerebrovascular diseases.

doi:10.6342/NTU202403077

1.4 Conclusions

This chapter provides an introduction to the fundamentals of the thesis, covering cerebral blood flow, its basic autoregulatory functions, and detailing the fundamental pathological characteristics of hypertension and ageing. We also briefly outline modern clinical methods, with a focus on the basic principles of the 4D flow MRI technique. We compare this technique with traditional MRI, particularly in terms of image quality and blood flow quantification, and elaborate on their respective advantages. Furthermore, the use of Transcranial Doppler (TCD) is discussed as an additional modality for assessing cerebral blood flow dynamics. We also consider the methods used to measure blood pressure, which is crucial for understanding the impacts of hypertension on cerebral autoregulation and assessing overall vascular health. These sections aim to provide a comprehensive overview of the imaging techniques and clinical measurements essential for the study of ageing and hypertension in relation to cerebral blood flow.

doi:10.6342/NTU202403077

Chapter 2

Models and Methods

This chapter explores the complex process of redeveloping cerebral blood flow autoregulation models, specifically to address the challenges posed by ageing and hypertension. It begins with a discussion on the multiscale model of cerebral autoregulation, designed to enhance our understanding and management of these conditions. Following this, the Cauchy stress tensor is introduced, with formulas derived and numerical methods applied to adapt the models for better accuracy in predicting the impacts of ageing and hypertension on cerebral autoregulation. Finally, the chapter introduces the haemodynamic model, incorporating the Cauchy stress tensor to establish a dynamic analysis that specifically accounts for changes in cerebral blood flow related to ageing and hypertensive conditions.

2.1 Multiscale Model of Cerebral Autoregulation

The autoregulatory mechanism, which helps maintain constant cerebral blood flow (CBF) despite changes in blood pressure, is a crucial factor to consider when analyzing diseases related to CBF. Therefore, accurately establishing this mechanism as a baseline

doi:10.6342/NTU202403077

condition is essential for effective disease analysis. This section will employ the multiscale model of cerebral autoregulation for its construction, encompassing four sub-models. These models are built upon physiological and chemical properties, with all parameters and formulas taken from [16].

2.1.1 Nitric Oxide Model

Among these four sub-models, the Nitric Oxide (NO) model is crucial; it specifically affects how the cerebral vasculature responds to conditions such as hypercapnia and hypoxia by regulating blood vessel dilation. NO, recognised as an endothelium-derived relaxing factor, is primarily produced by endothelial nitric oxide synthase (eNOS) within endothelial cells and plays a significant role in metabolism. In this study, NO concentration is a key parameter. We assume that NO is present in the blood and vessel walls of small arteries, and the concentration of NO in the blood can be spatially averaged. Therefore, after defining the vessel-average concentration of NO, it can be determined using linear algebra operations:

$$\overline{C_b} = \left(\frac{h_w C_{w_e}}{h_w + r_{db}A_b} - C_{in}\right)\left(1 - \frac{Q}{(h_w + r_{db}A_b)L}\left(1 - e^{-(h_w + r_{db}A_b)\frac{L}{Q}}\right)\right) + C_{in} \qquad (1)$$

doi:10.6342/NTU202403077

where C_{in} is the bloodstream's inlet NO concentration, h_w is the blood diffusion proportionality constant from the vessel wall, C_{we} is the vessel wall's effective NO concentration, r_{db} is the blood's rate at which NO degrades, A_b is the vessel lumen's cross-section. This is based on the assumption that the concentration is in quasi-steady-state.

In this study, the concentration of NO significantly influences the concentration of cGMP ([cGMP]), thus we establish their relationship using the following equation (Figure 2.1):

$$p[cGMP] = p[cGMP]_L + \frac{p[cGMP]_U - p[cGMP]_L}{1 + e^{-\frac{[NO]-z_{half}}{k_z}}} \tag{2}$$

where

$$z_{half} = [NO]_L + \frac{[NO]_U - [NO]_L}{2} \qquad k_z = \frac{[NO]_L - [NO]_U}{2\ln\left(\frac{1}{0.95} - 1\right)} \tag{3}$$

doi:10.6342/NTU202403077

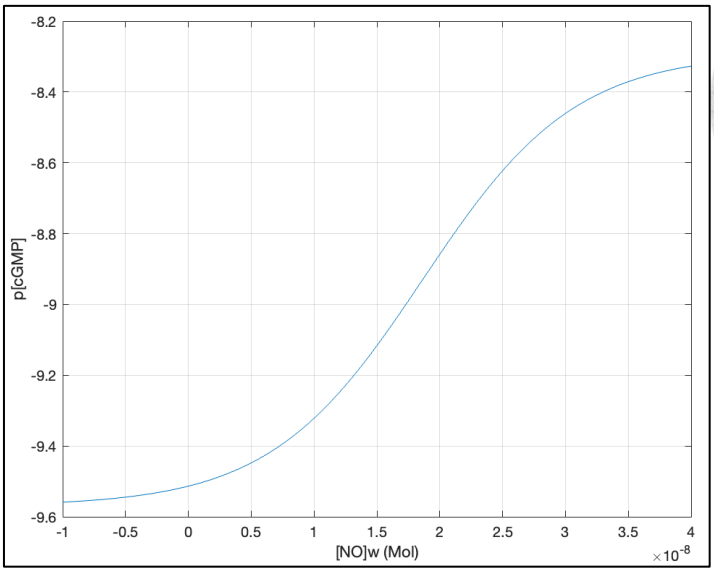

Figure 2.1 The relationship between [NO] and p[cGMP]. (Figure reproduced from [17]).

2.1.2 Simplified Myogenic Response Model

In the myogenic response model [18], it is assumed that myogenic responsiveness is solely sensitive to circumferential stress on the vessel wall and is influenced only by the concentration of calcium ions. Consequently, we employ a descriptive approach similar to that used for NO and cGMP to define the effects of calcium ion concentration and vessel wall stress:

$$p\overline{[Ca^{2+}]} = p[Ca^{2+}]_L + \frac{p[Ca^{2+}]_U - p[Ca^{2+}]_L}{1 + e^{-\frac{\sigma - z_{half}}{k_z}}} \quad (4)$$

doi:10.6342/NTU202403077

where the σ is vessel wall stress and the functions of $p\overline{[Ca^{2+}]}$, z_{half} and k_z are:

$$z_{half} = \sigma_L + \frac{\sigma_U - \sigma_L}{2} \qquad k_z = \frac{\sigma_L - \sigma_U}{2\ln\left(\frac{1}{0.95} - 1\right)} \tag{5}$$

Further, by introducing the formula from Section 2.1.1, we can establish the relationship between rPhosphorylation and Ca^{2+} (Figure 2.2).

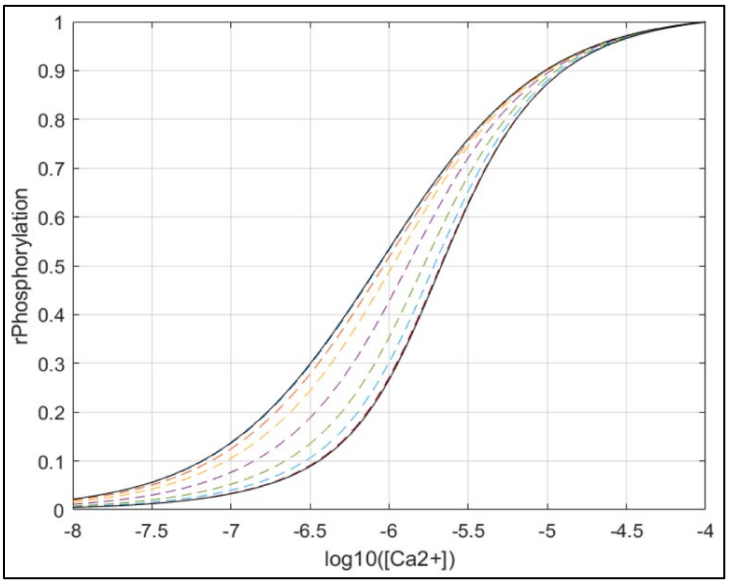

Figure 2.2 The upper and lower black solid lines represent the data of concentrations of [8Br-cGMP] are 0M and 2μM. (Figure reproduced from [17]).

doi:10.6342/NTU202403077

2.1.3 4-State Kinetic Model

This model uses a kinetic model [19] to describe the interaction between cross-bridges and actin filaments in smooth muscle. It consists of four elements: unphosphorylated cross-bridge M, phosphorylated cross-bridge M_p, phosphorylated and attached cross-bridge AM_p , and unphosphorylated and attached cross-bridge AM, with their relationships being:

$$M + M_p + AM_p + AM = 1 \tag{6}$$

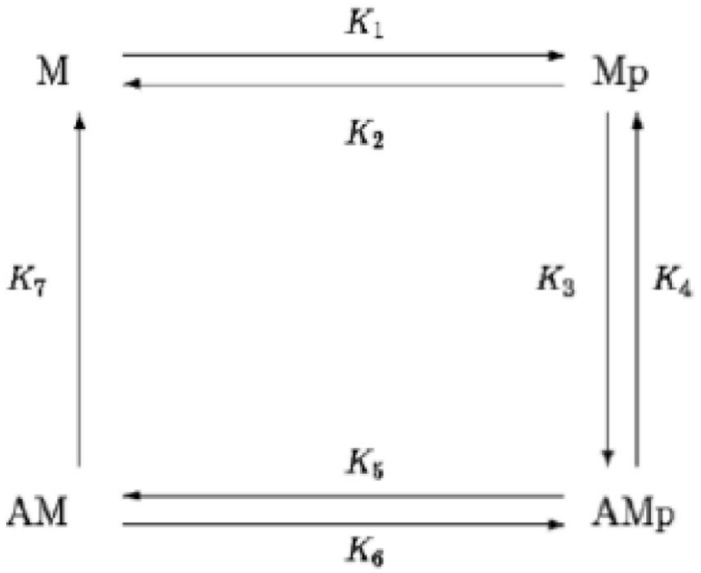

Figure 2.3 The 4-state kinetic model. (Figure reproduced from [19]).

Then introduce their seven rate constants K, assuming they are directly related only to the concentration of calcium ions, and under steady-state conditions:

doi:10.6342/NTU202403077

$$\begin{bmatrix} M \\ Mp \\ AMp \\ AM \end{bmatrix} = \begin{bmatrix} -K_1 & K_2 & 0 & K_7 \\ K_1 & -K_2 - K_3 & K_4 & 0 \\ 0 & K_3 & -K_4 - K_5 & K_6 \\ 1 & 1 & 1 & 1 \end{bmatrix} \cdot \begin{bmatrix} 0 \\ 0 \\ 0 \\ 1 \end{bmatrix} \quad (7)$$

where K_1 and K_6 are phosphorylation rates can be calculated by $[Ca^{2+}]$, K_2 and K_5 are dephosphorylation rates can be calculated by $[Ca^{2+}]$ and $[cGMP]$, K_3, 、K_4 and K_7 are the rate constants for the following processes: non-phosphorylated detachment, phosphorylated attachment, and phosphorylated detachment. Through the above formula, we can obtain the value of AM_p and introduce it to the subsequent Mechanical Model.

2.1.4 Mechanical Model

In the study by [20], a biophysical explanation for the electrical, chemical, and mechanical phenomena in cerebral vascular smooth muscle is provided. Therefore, it can be assumed that the mechanical model can be divided into active force F_a:

$$F_a = l_0\left(f_1 AM_p\left(\hat{v} + \dot{\lambda}\right) + f_2 AM\dot{\lambda}\right)e^{-\left(\lambda-\lambda_{opt}\right)^2} \quad (8)$$

where l_0 is the vascular smooth muscle cells' relaxed length, f_1 and f_2 are the coefficients of viscous friction for AM_p and AM respectively, $\hat{v}$ is the standard cycling speed across a bridge, λ is the length of the normalized cell, $\dot{\lambda}$ is the

doi:10.6342/NTU202403077

derivative in time of λ, and λ_{opt} is the cell length normalized in the maximum overlap scenario.

Originating from actin-myosin filaments and overlapping actomyosin, and passive force F_p coming from the unit passive stiffness, is defined as:

$$F_p = q_1\left(e^{q_2(\lambda-1)} - 1\right) \tag{9}$$

where q_1 and q_2 are stiffness coefficients.

Hence, in this model, the total force is F_T defined as:

$$F_T = F_a + F_p \tag{10}$$

Using mathematical model analysis [21], the above formula can be further derived as:

$$0 = q_1\left(e^{q_2(\lambda q_3-1)} - 1\right) + l_0 f_1 AMp\hat{v}e^{\frac{-(\lambda-\lambda_{opt})^2}{2\eta}} - w_c P\frac{1}{2}\left(\frac{\lambda l_0 n_c}{\pi} - t_w\right) \tag{11}$$

where q_3 is stiffness coefficient, η is modification coefficient, w_c is the width of the single cell, n_c is the number of cells and t_w is the thickness of the vessel wall.

Since the above formula is a nonlinear function related to vascular pressure, the vessel radius can be further determined using Newton's method [22] or numerical

doi:10.6342/NTU202403077

methods, more detailed flowchart will be introduced in Section 3.1.

2.2 Cauchy Stress Tensor

The original model of cerebral autoregulation, when applied to cerebral blood flow analysis, involves a highly complex array of parameters and equations. Therefore, we utilize the Cauchy Stress Tensor [23] as the basis for remodelling. The importance of this approach lies in its ability to provide a comprehensive mathematical framework that captures the mechanical properties of cerebral tissues under varying physiological conditions [47]. This is crucial for accurately simulating how the brain's structure responds to different stressors, which is essential for developing more effective treatments and understanding various cerebral conditions. Compared to the earlier model, this new approach significantly reduces the number of parameters and equations needed [47], enhancing flexibility for calculating both vessel radius and blood pressure. Importantly, it offers a comprehensive framework for remodeling that effectively addresses both slow and rapid changes in one unified model. This section will introduce the fundamental components of the formula as well as the basic assumptions and simplifications

doi:10.6342/NTU202403077

involved.

2.2.1 Introduction

The Cauchy Stress Tensor is a pivotal mechanical model in continuum mechanics for analysing internal forces within a system, represented using Eulerian variables. In this study, it is formulated in terms of arterial mechanics, allowing for the control and analysis of physical quantities within human blood vessels. Thus, in arterial mechanics, the form of the Cauchy Stress Tensor is as follows:

$$\boldsymbol{t}(s) = -p(s)\mathbf{I} + \frac{2}{\boldsymbol{J}(s)}\mathbf{F}(s)\frac{\partial W_R}{\partial \boldsymbol{C}(s)}\mathbf{F}^{\mathrm{T}}(\mathrm{s}) + \mathbf{t}^{\mathrm{act}}(\mathrm{s}) \qquad (12)$$

where $p(s)$ is a Lagrange multiplier, $\mathbf{I}$ is the identity tensor, $\mathbf{F}(s)$ is the deformation gradient tensor (Figure 2.4) which detailed visualization aids in understanding the aorta's mechanical response to different physiological and pathological states, such as ageing and hypertension, and highlights the importance of accurate modeling for effective analysis and treatment. $\boldsymbol{J}(s)$ is a volumetric ratio, $\boldsymbol{C}(s)$ is the right Cauchy–Green tensor, W_R is a strain-energy function and $\mathbf{t}^{\mathrm{act}}(\mathrm{s})$ is the active stress generated by smooth muscle [24,25].

doi:10.6342/NTU202403077

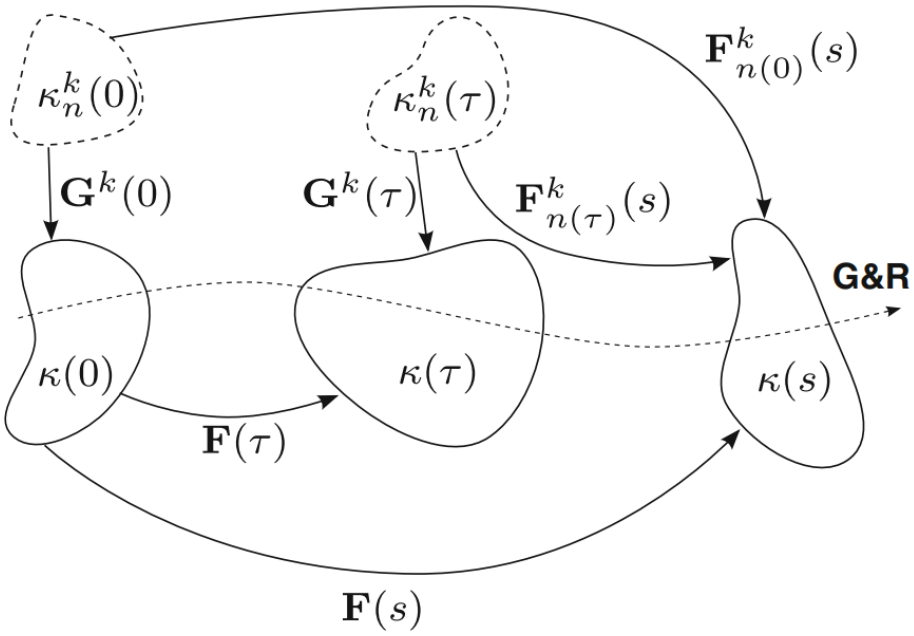

Figure 2.4 The deformation gradient tensors across different states of blood vessel (in vivo, excised, and radially cut). (Figure reproduced from [25]).

2.2.2 Assumptions and Simplifications

In the mechanical analysis of blood vessels, we assume that the flow rate changes sufficiently slowly over time, the vessel walls do not change under stress, the load is symmetrically distributed along the vessel's axis, and the strain across the vessel cross-section is consistent at all sections. Therefore, we list four assumptions for subsequent analysis in this study:

doi:10.6342/NTU202403077

1.Quasi steady-state conditions ($\frac{\partial}{\partial s} = 0$)

2.Vessel wall incompressibility ($\boldsymbol{J} = 1$)

3.Axisymmetric loading ($\frac{\partial}{\partial \theta} = 0$)

4.Plane strain conditions ($\lambda_z = 1$)

These four assumptions allow us to avoid complex dynamic analysis, eliminate the need to consider changes in the volume of the vessel wall, use a simpler cylindrical coordinate system for analysis, and reduce the problem from three dimensions to one. While this significantly simplifies computational complexity, we will discuss their limitations in this study in Chapter 4.

Therefore, the Cauchy Stress Tensor can be simplified to:

$$\boldsymbol{t} = -p\mathbf{I} + 2\mathbf{F}\frac{\partial W_R}{\partial \boldsymbol{C}}\mathbf{F}^{\mathrm{T}} + \mathbf{t}^{\mathrm{act}} \tag{13}$$

The W_R can be simplified in:

$$W_R = \sum_k \emptyset^k \, \widehat{W}^k \tag{14}$$

where:

$$\widehat{W}^e = \frac{c^e}{2}\{tr(\mathbf{F}^T\mathbf{F}) - 3\} \tag{15}$$

doi:10.6342/NTU202403077

$$\widehat{W}^{c,m} = \frac{c_2^{c,m}}{4c_3^{c,m}}\left\{\exp\left(c_3^{c,m}\left[\frac{1}{3}tr(\mathbf{F}^T\mathbf{F}) - 1\right]^2\right) - 1\right\} \quad (16)$$

Because the assumption, **F** can be reduced in:

$$\mathbf{F} = \text{diag}\left[\frac{\partial r}{\partial r(0)} \quad \frac{r}{r(0)} \quad 1\right] \quad (17)$$

where:

$$r^2 = r^2(0) - r_i^2(0) + r_i^2 \quad (18)$$

The $\mathbf{t}^{\text{act}}$ can be reduced in:

$$\mathbf{t}^{\text{act}} = T_{max}\phi^m[1 - exp(-C^2)]\lambda_\theta^{m(act)}\left[1 - \left(\frac{\lambda_M - \lambda_\theta^{m(act)}}{\lambda_M - \lambda_0}\right)^2\right] \quad (19)$$

where

$$C = C_B - C_S\left(\frac{\tau_w}{\tau_w^h} - 1\right) \quad (20)$$

and

$$\tau_w = \frac{4\mu Q}{\pi a^3} \quad (21)$$

This can be replaced by the pressure drop using the Hagen-Poiseuille equation.

$$Q = \frac{\pi r^4}{8\mu L} \cdot \Delta P \quad (22)$$

doi:10.6342/NTU202403077

If we disregard p, then the eqn.11 becomes:

$$\boldsymbol{t} = 2\frac{\partial W_R}{\partial I_1}\mathbf{B} - \frac{2}{3}I_1\frac{\partial W_R}{\partial I_1}\mathbf{I} + \mathbf{t}^{\text{act}} \tag{23}$$

where **B** is the right Cauchy–Green tensor, $I_1 = tr(\mathbf{F}^T\mathbf{F})$.

Finally, through the equilibrium equation [26]:

$$\frac{\partial t_{rr}}{\partial r} = \frac{t_{\theta\theta} - t_{rr}}{r} \tag{24}$$

Hence

$$P_i - P_a = \int_{r_i}^{r_a} \frac{t_{\theta\theta} - t_{rr}}{r}\, dr \tag{25}$$

where $P_i - P_a$ is current transmural pressure.

For a given pressure difference, the internal wall pressure (internal minus external) and pressure drop (inlet minus outlet) can be determined using the equilibrium equation in conjunction with numerical integration to calculate the internal radius of the vessel (these are set in the same way as set out in section 2.3).

doi:10.6342/NTU202403077

2.2.3 Parameters Adjustment

In the new mathematical model, in order to align with the reestablishment of cerebral blood flow autoregulation, we have recalibrated the following parameters (Table 2.1) in this study.

Parameters	Value	Unit
$\emptyset^e$	0.55	
$\emptyset^c$	0.25	
$\emptyset^m$	0.2	
r_0	6	μm
λ_M	2	
λ_0	0.4	
C_B	0.68	
τ_w^h	0.5	Pa
T_{max}	300	kPa
C^e	125	kPa

Table 2.1 The values in Cauchy stress tensor. (Values reproduced from [25]).

Here $\emptyset^e$、$\emptyset^c$ are medial constitutive fractions and $\emptyset^m$ is the evolving mass fraction of active smooth muscle [26], r_0 represents the radius in the standard type, λ_M、λ_0 and T_{max} are vasoactivity [27], C_B is shear-constrictor [28], τ_w^h is initial load [29], C^e is

doi:10.6342/NTU202403077

passive elasticity.

2.2.4 Progressive Vasoactive Dysfunction

To observe cerebral blood flow autoregulation across different age groups, we have set T_{max} to vary over time, therefore:

$$T_{\max}(s) = [(1 - \beta_m)e^{-K^e s} + \beta_m]T_{\max}(0) \tag{26}$$

where $\beta_m = 0.75$ is a scaling parameter that controls the degree of proportionality between elastin content and vasoactivity, $K^e = \ln(2) / 14600\ \text{day}^{-1}$ [30] is crucial as it quantifies the rate of elastin degradation in the arteries, which is fundamental for modeling how arterial stiffness increases over time, particularly due to ageing and hypertension

doi:10.6342/NTU202403077

2.3 Haemodynamic Model

To provide a clear foundation for understanding the haemodynamic model (Figure 2.4), it is essential to describe its core concepts first. This model, which is designed to enhance previous vascular analyses, simulates the vascular tree by drawing analogies with electrical circuit models. In this framework, all individual arteries and arterioles are assumed to respond to pressure changes by adjusting their diameters uniformly. Within the model, blood pressure and flow correlate with voltage and current, respectively, offering an intuitive way to comprehend the dynamic behaviors of cerebral blood flow.

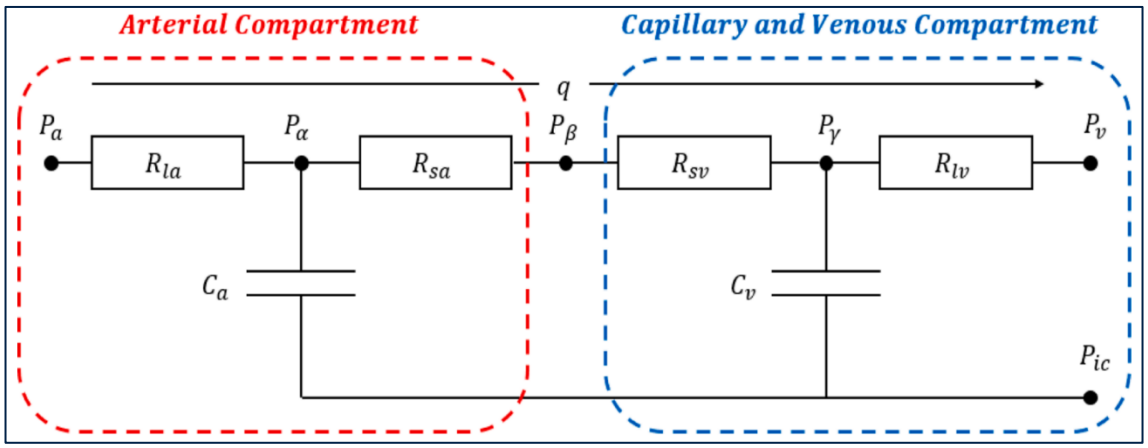

Figure 2.5 The whole-brain vasculature model. (Figure reproduced from [17]).

doi:10.6342/NTU202403077

2.3.1 Steady state

Since the flow q in every section of the circuit is constant under steady-state circumstances, Kirchhoff's law can be used as follows:

$$q = \frac{P_a - P_v}{R_{la} + R_{sa} + R_{lv} + R_{sv}} \tag{27}$$

where P_a is the systemic arterial pressure, P_v is the blood pressure, R_{la} and R_{sa} are the corresponding resistance of the regulating and non-regulating artery sections, R_{lv} and R_{sv} are the capillary & small vein compartment and big vein resistances, respectively. According to the Hagen-Poiseuille equation, the R_{sa} is given by:

$$R_{sa} = \frac{8\mu_b L}{\pi r^4 n_{sa}} \tag{28}$$

where n_{sa} is the effective number of parallel arterioles in the vascular tree, L is characteristic length of arterioles, μ_b is blood viscosity.

Finally, by adding the vessel radius, which is calculated using the Section 2.1 original model, combined with the flowchart (introduced in Section 3.1) and the numerical methods (introduced in Section 2.4) into this formula, one can obtain the relationship for cerebral blood flow autoregulation.

doi:10.6342/NTU202403077

2.3.2 Dynamic state

The flow in each circuit changes over time, thus by Kirchhoff's law, governing equations for venous pressure and upstream arteriolar pressure can be established:

$$\frac{dP_\alpha}{dt} = \frac{1}{C_a}\frac{dC_a}{dt}(P_\alpha - P_{ic}) + \left(\frac{P_a - P_\alpha}{R_{la}} + \frac{P_\beta - P_\alpha}{R_{sa}}\right)\frac{1}{C_a} \tag{29}$$

$$\frac{dP_\gamma}{dt} = \frac{1}{C_v}\frac{dC_v}{dt}\left(P_\gamma - P_{ic}\right) + \left(\frac{P_\beta - P_\gamma}{R_{sv}} + \frac{P_v - P_\gamma}{R_{lv}}\right)\frac{1}{C_v} \tag{30}$$

where P_α and P_β are the pressures upstream and downstream of the arteriolar level respectively, P_γ is venous pressure, P_{ic} is intracranial pressure, C_a and C_v are the arterial and venous compliances, which can be defined as:

$$C_a = \frac{1}{k_{art}(P_\alpha - P_{ic} - P_{a1})} \tag{31}$$

$$C_v = \frac{1}{k_{ven}(P_\gamma - P_{ic} - P_{v1})} \tag{32}$$

where k_{art} and k_{ven} are the stiffness coefficients for arterial and venous compliance respectively, P_{a1} and P_{v1} are the pressure offsets for arterial and venous compliance respectively.

doi:10.6342/NTU202403077

Also, there is a relationship between pressure:

$$P_\beta = P_\gamma + \frac{R_{sv}}{R_{sa} + R_{sv}}\left(P_\alpha - P_\gamma\right) \tag{33}$$

and the following initial conditions:

$$q(0) = \frac{P_a(0) - P_v}{R_{la} + R_{sa}(0) + R_{lv} + R_{sv}} \tag{34}$$

$$P_\alpha(0) = P_a(0) - q(0)R_{la} \tag{35}$$

$$P_\beta(0) = P_a(0) - q(0)(R_{la} + R_{sa}(0)) \tag{36}$$

$$P_\gamma(0) = P_a(0) - q(0)(R_{la} + R_{sa}(0) + R_{sv}) \tag{37}$$

Subsequently, by employing numerical methods (introduced in Section 2.4), we can determine the dynamic conditions of pressure, vessel radius, and blood flow rate. It's important to note that the inputs to this model include arterial and venous pressures as functions of time, which are crucial for accurately simulating the physiological changes occurring within the cerebral vasculature.

doi:10.6342/NTU202403077

2.4 Numerical Methods

In this study, we extensively use MATLAB's functions to perform our analyses, focusing on essential analytical methods [31]. We start with the fzero function to accurately determine the vessel radius in the multiscale model of cerebral autoregulation [32]. This is crucial for establishing the relationship in cerebral blood flow autoregulation. Next, we use the Optimization toolbox to adjust parameters within the Cauchy Stress Tensor, critical for our remodelling work. This adjustment is important for correctly establishing autoregulation curves and for accurately calculating differences between models. This optimization phase includes using regression analysis techniques from machine learning, specifically gradient descent methods [33], to find the minimum square error and identify necessary parameter adjustments. Lastly, we use the ODE 45 function, which applies the advanced 45th order Runge–Kutta method [34, 35] for numerical integration, to develop dynamic monitoring change curves for cerebral blood flow. This section aims to provide a clear explanation of how we implemented these methods, ensuring that the analysis is comprehensive and accessible.

doi:10.6342/NTU202403077

2.5 Conclusions

This chapter describes numerous complex models and the physical significance behind their parameters. Besides analytical tools, it also emphasizes the importance of analysing the properties of CBF and CBF autoregulation curves as baseline values, which hold significant implications in the analysis of cerebrovascular diseases. We will generate the results in both the steady and dynamic states in the next chapter.

doi:10.6342/NTU202403077

Chapter 3

Results and Discussions

In this chapter, we will present the findings outlined in the previous chapter. These findings are divided into three sections: results of the original model in steady state, results of the new mathematical model in steady state, and results of the new model in dynamic state. We will concentrate primarily on the results of the dynamic state in this section, with a particular emphasis on the changes in blood flow and vessel radius over time. The implications of these findings will be discussed further in the next section.

3.1 Results of Original Model in Steady State

In this section, we will establish the steady state values for blood vessel radius and the curve for cerebral blood flow autoregulation, which will facilitate subsequent remodelling and serve as initial condition parameters for the dynamic state.

doi:10.6342/NTU202403077

3.1.1 Steady State Blood Vessel Radius

We introduced the nitric oxide model, simplified myogenic response model, 4-state kinetic model, and mechanical model in Section 2.1. Here, we will use the procedure shown in (Figure 3.1) in conjunction with the fzero function (introduced in Section 2.4) to establish the blood vessel radius corresponding to the systemic arteriolar pressure under steady state conditions (Figure 3.2).

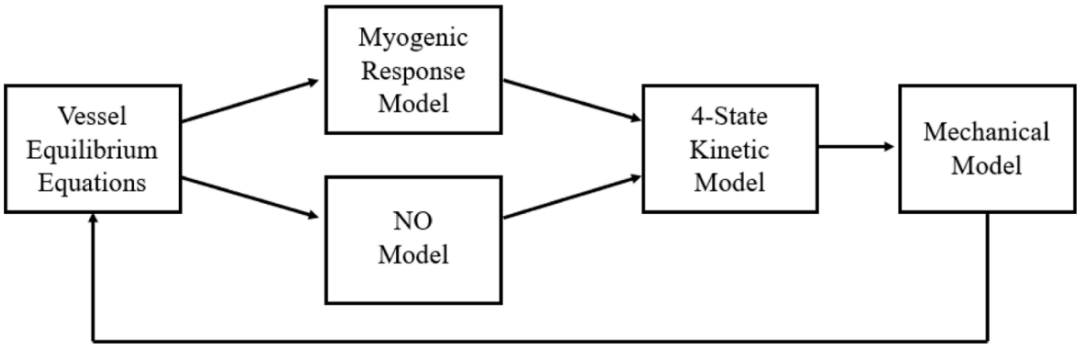

Figure 3.1 The flowchart of original model. (Figure reproduced from [16]).

doi:10.6342/NTU202403077

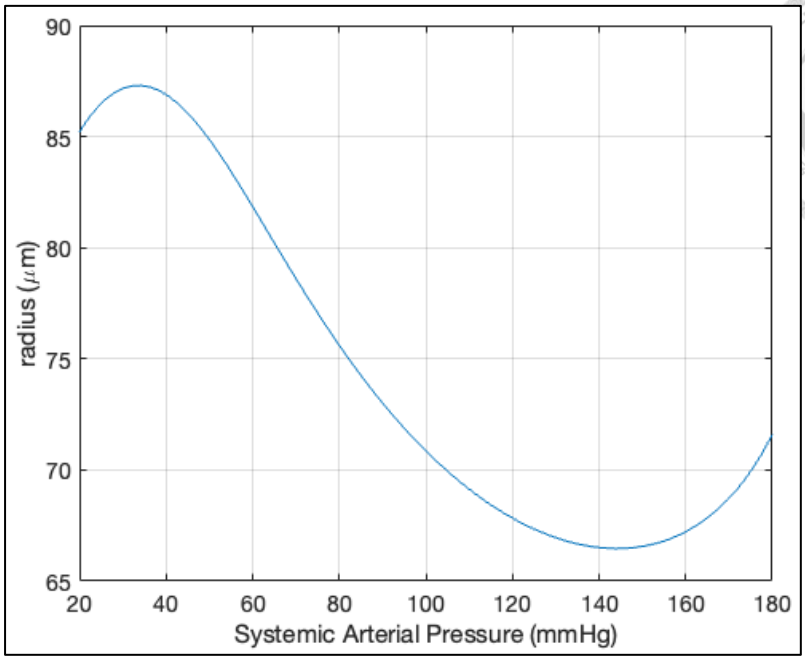

Figure 3.2 Radius vs systemic arterial pressure by using the steady state haemodynamic model shows the changes in the vessels under conditions with flow.

3.1.2 Steady State CBF Autoregulation

The results are consistent with those presented in [36], thereby successfully using the original model to establish the steady state values of blood vessel radius. Previously in Section 2.3.1, used the haemodynamic model along with Hagen-Poiseuille's equation to establish mathematical expressions for blood flow, resistance, and systemic arteriolar pressure. Since R_{sa} varies with the blood vessel radius, by introducing the blood vessel radius values established by the original model, we can obtain the curve for cerebral

doi:10.6342/NTU202403077

blood flow autoregulation under steady state conditions (Figure 3.3).

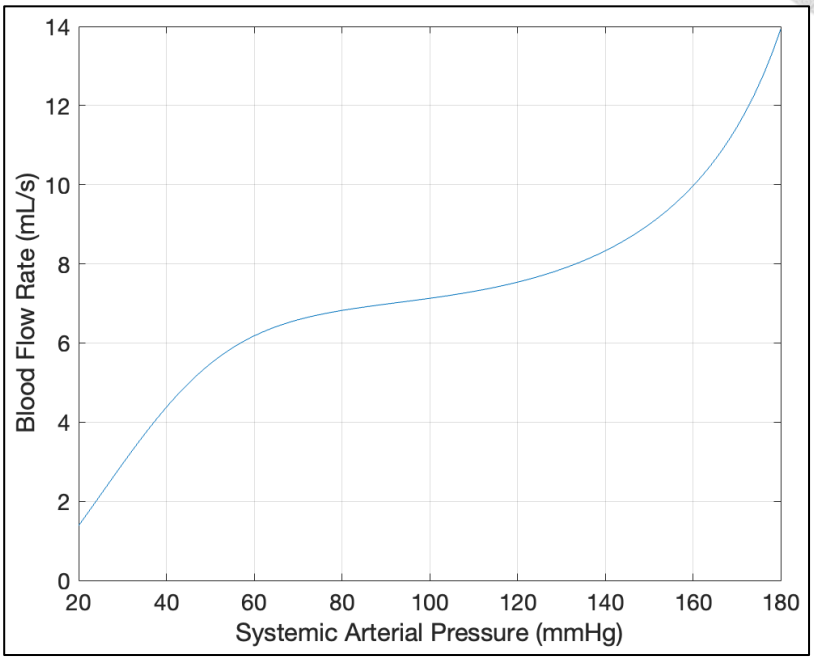

Figure 3.3 Steady state blood flow rate vs systemic arterial pressure by using the steady state haemodynamic model, we validated this model using data from rats and cats as documented in [37].

The autoregulation curve's trend aligns with our expectations, suggesting our model's accuracy, which can be further confirmed using data from [37]. However, it is important to note that the primary focus of this study is on developing the model itself rather than extensive empirical validation.

doi:10.6342/NTU202403077

Due to the complexity caused by the numerous parameters in our current model, we will introduce a new mathematical model in the next section to streamline our approach.

3.2 Results of New Mathematical Model in Steady State

In this section, we will use a new mathematical model to replace the existing one, using numerical methods to re-establish the curve for cerebral blood flow autoregulation. We will then incorporate progressive vasoactive dysfunction to observe trends in cerebral blood flow autoregulation across different age groups.

3.2.1 Optimization

The original model, due to the excessive number of parameters, is now replaced with a new mathematical model. We use the Cauchy stress tensor (simplified in Section 2.2.2) along with MATLAB optimization toolbox for parameter fitting (mentioned in Section 2.2.3). However, due to interval limitations and constraints on some parameters, we will use the fmincon function [38] for parameter fitting. The fmincon function in MATLAB is an optimization solver that minimizes a constrained nonlinear multivariable function, effectively aiding in the accurate adjustment of our model's parameters to better fit the

doi:10.6342/NTU202403077

data. The intervals for the parameter fitting, as depicted in Table 3.1, are chosen based on their role as the upper and lower bounds where the model outputs begin to diverge, ensuring the stability and reliability of the simulation results.

Parameters	Upper Band	Lower Band	Result	Unit
$\emptyset^e$	0.80	0.75	0.76	
$\emptyset^c$	0.20	0.10	0.12	
$\emptyset^m$	0.20	0.10	0.12	
r_0	6.5	6	6.49	μm
λ_M	1.5	1	1.49	
λ_0	3	1.2	1.81	
C_B	0.0025	0.002	0.0022	
τ_w^h	20	0.5	1.19	Pa
T_{max}	301	290	300	kPa
C^e	70	62	62.5	kPa

Table 3.1 The fitting interval and results of parameters.

After fitting, we use the least squares method to observe an error value ($loss = 4.0618\ mmHg \cdot mL/s$), which is very small [35]. We further examined the autoregulation curves generated by the two models (Figure 3.4). The main discrepancies occurred in the lower-pressure part, but these differences are within the range of experimental error commonly seen in measurements, making them acceptable. In this

doi:10.6342/NTU202403077

study, our primary focus is on the midsection's flat line segment; thus, we can directly utilize the new mathematical model for subsequent dynamic analysis.

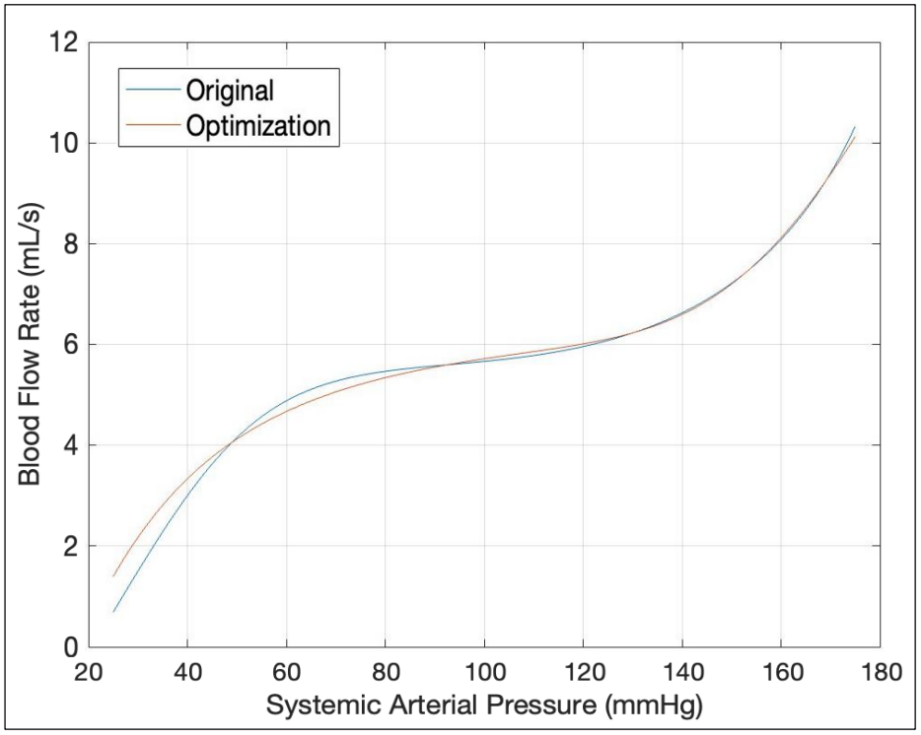

Figure 3.4 The difference between original model and new mathematic model.

3.2.2 Progressive Vasoactive Dysfunction

As proposed in Section 2.2.4, T_{max} which represents the maximum tension the vessel wall can withstand, changes with age. This change is due to the physiological alterations in vascular elasticity and strength that occur as part of the ageing process, making it crucial to adjust this parameter in models analyzing age-related vascular changes. Here,

doi:10.6342/NTU202403077

we introduce it into the autoregulation curve from Section 3.2.1, with the T_{max} at age 20 as the baseline condition because this is when an individual's cardiovascular system is fully developed, offering a standard reference for assessing changes due to ageing or disease. Following equation 26, we can establish the autoregulation curve up to age 100 (Figure 3.5). It is observed that the low-pressure part trend changes, but the trends in the high-pressure part eventually converge. Thus, using the new mathematical model, we can further observe the trends in blood flow during ageing.

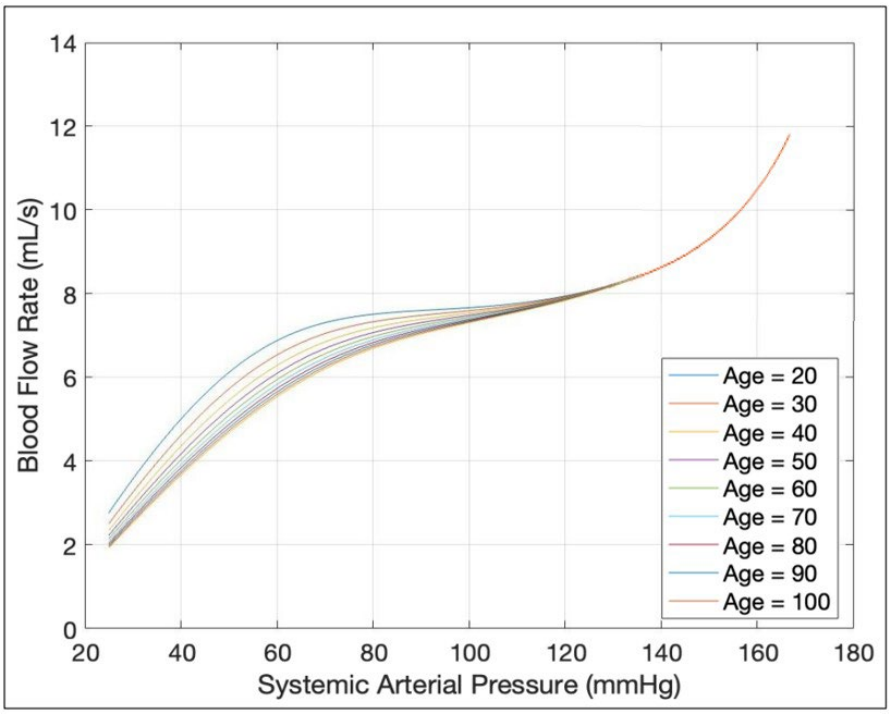

Figure 3.5 The CBF autoregulation in different years by using the progressive vasoactive dysfunction, this is because as age increases, the elasticity of the vascular

doi:10.6342/NTU202403077

walls gradually decreases, reducing the reactivity of the vessels under low pressure conditions.

3.3 Results of Dynamic State

In this section, we will employ the optimized new mathematical model, in conjunction with the methods mentioned in Sections 2.3.2 and 2.4, to establish the dynamic state. We will then introduce progressive vasoactive dysfunction to observe the blood flow and vessel radius dynamics across different age groups.

3.3.1 The Results of Dynamic State

Using the integral formulas and numerical methods previously mentioned, and setting a sudden increase or decrease in systemic arterial pressure at the zero with a pressure difference of 10% (between 72 and 80), we can see the vessel radius values under dynamic conditions in Figures 3.6 and 3.7.

doi:10.6342/NTU202403077

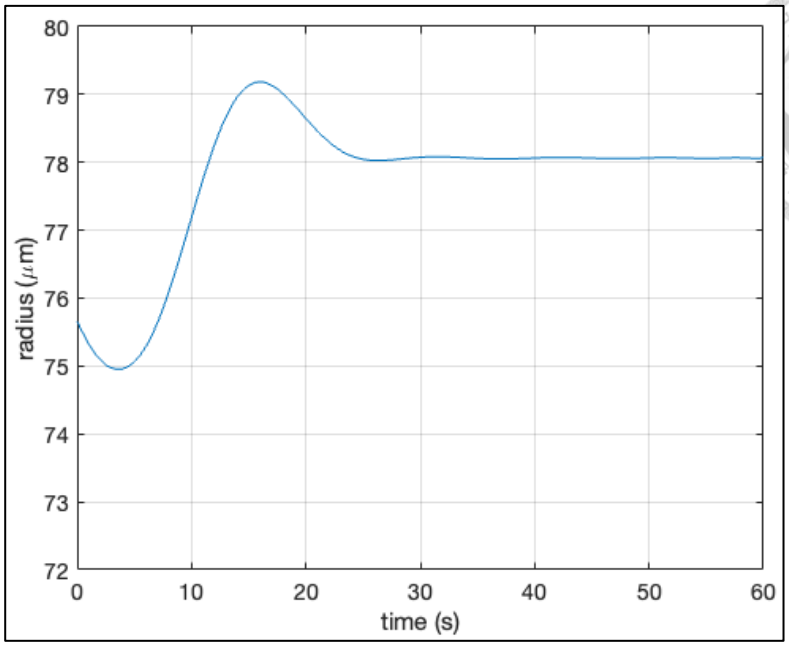

Figure 3.6 Dynamic radius for pressure drop from $P_a = 80\ mmHg$ to $72\ mmHg$.

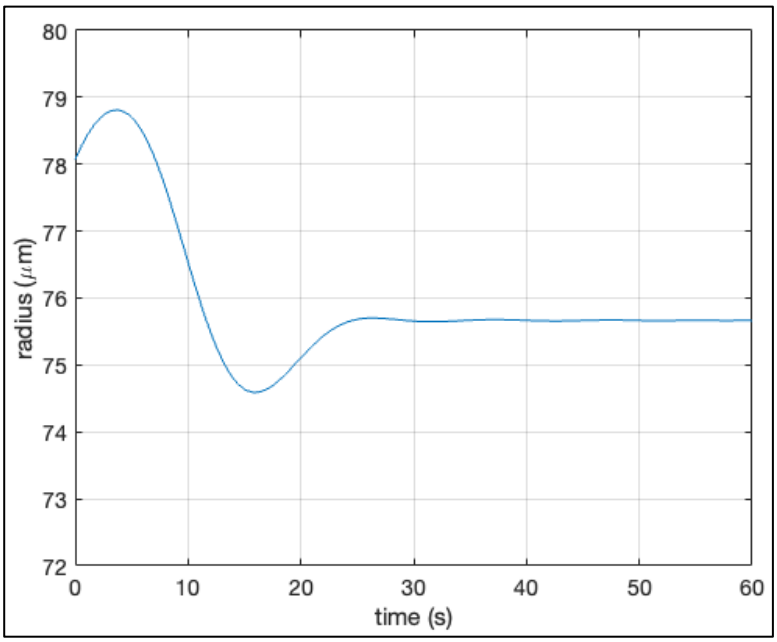

Figure 3.7 Dynamic radius for pressure rising from $P_a = 72\ mmHg$ to $80\ mmHg$.

From the results shown in the figures, the trend in vessel radius under dynamic

doi:10.6342/NTU202403077

conditions matches those found in previous studies (Figure 3.8), allowing us to further observe the blood flow as shown in Figures 3.9 and 3.10.

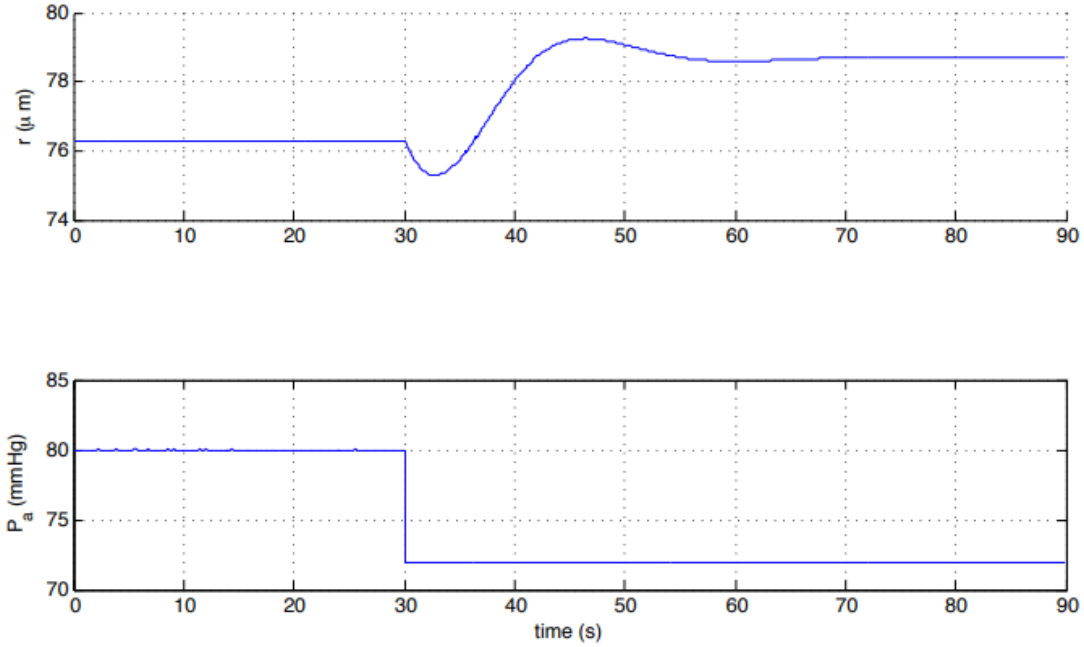

Figure 3.8 Dynamic radius for pressure drop from $P_a = 80\ mmHg$ to $72\ mmHg$ in the original study (Figure reproduced from [17]). This result exhibits the same trend as our fitted results.

doi:10.6342/NTU202403077

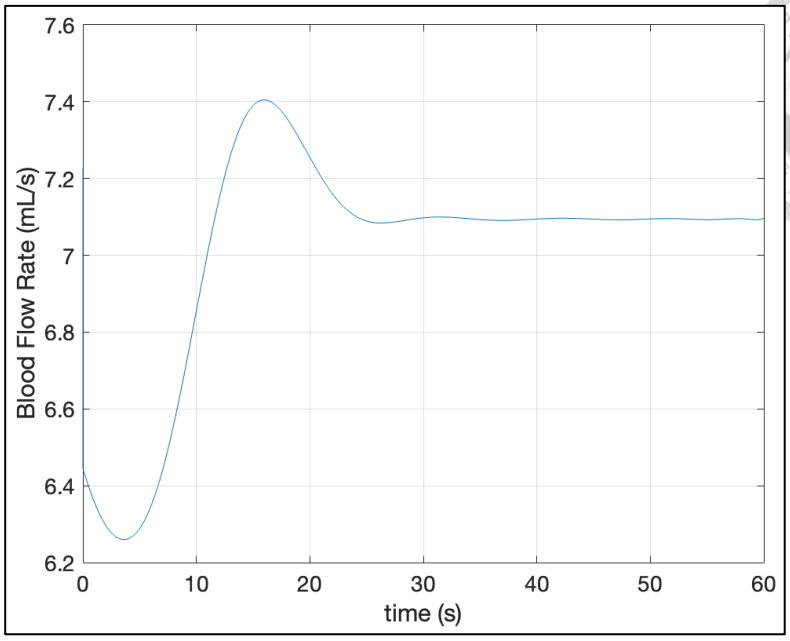

Figure 3.9 Dynamic flow rate for pressure drop from $P_a = 80\ mmHg$ to $72\ mmHg$.

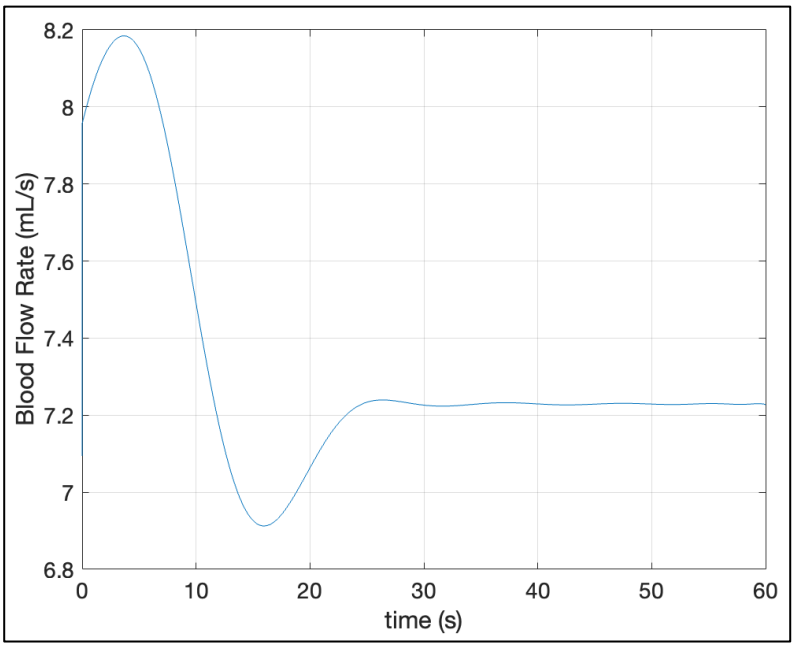

Figure 3.10 Dynamic flow rate for pressure rising from $P_a = 72\ mmHg$ to $80\ mmHg$.

doi:10.6342/NTU202403077

The graphs show that the trend in blood flow under dynamic conditions also aligns with previous studies (Figure 3.11), with the graphs of pressure increase and decrease maintaining symmetry which is due to cerebral autoregulation adjusting vascular resistance to maintain near constant blood flow despite fluctuations in blood pressure.

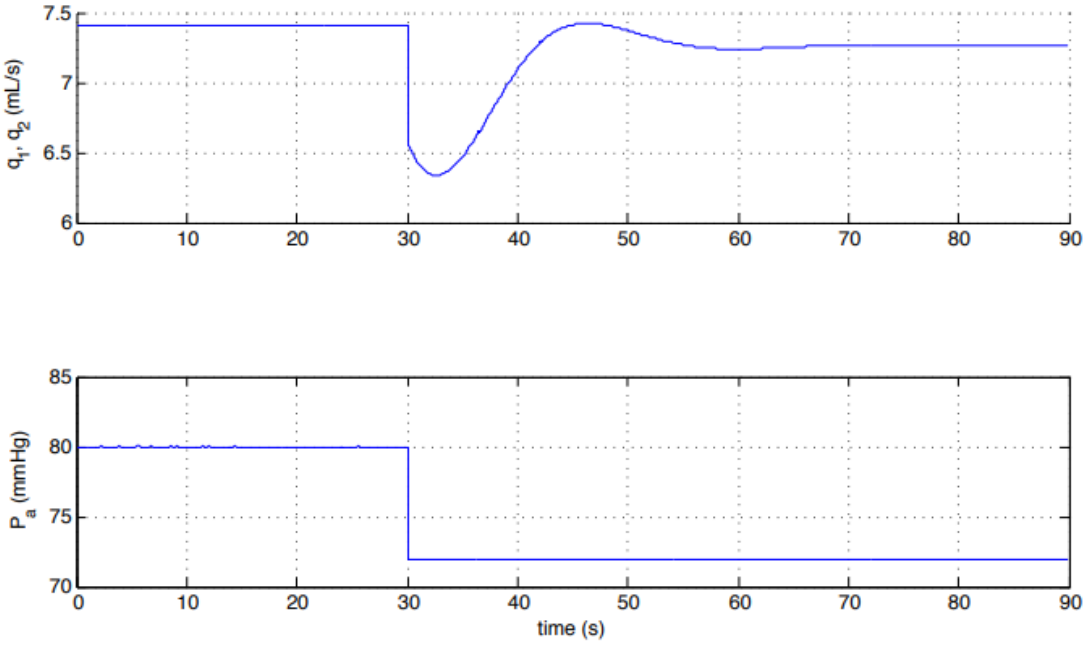

Figure 3.11 Dynamic flow rate for pressure drop from $P_a = 80\ mmHg$ to $72\ mmHg$ in the original study (Figure reproduced from [17]). This result exhibits the same trend as our fitted results.

doi:10.6342/NTU202403077

3.3.2 Progressive Vasoactive Dysfunction

Similar to Section 3.2.2, we introduce T_{max} into the dynamic state to observe changes in vessel radius and blood flow across different ages. As shown in Figures 3.12 and 3.13, We observe the trends in vessel radius under dynamic conditions across different age groups, noting that both the initial and final values differ due to changes in baseline conditions associated with ageing.

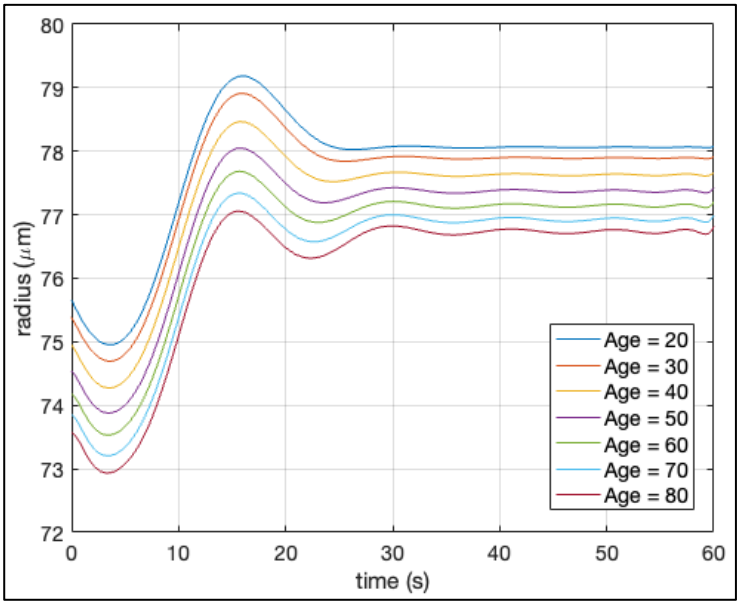

Figure 3.12 Dynamic radius for pressure drop from $P_a = 80\ mmHg$ to $72\ mmHg$ follow the different ages.

doi:10.6342/NTU202403077

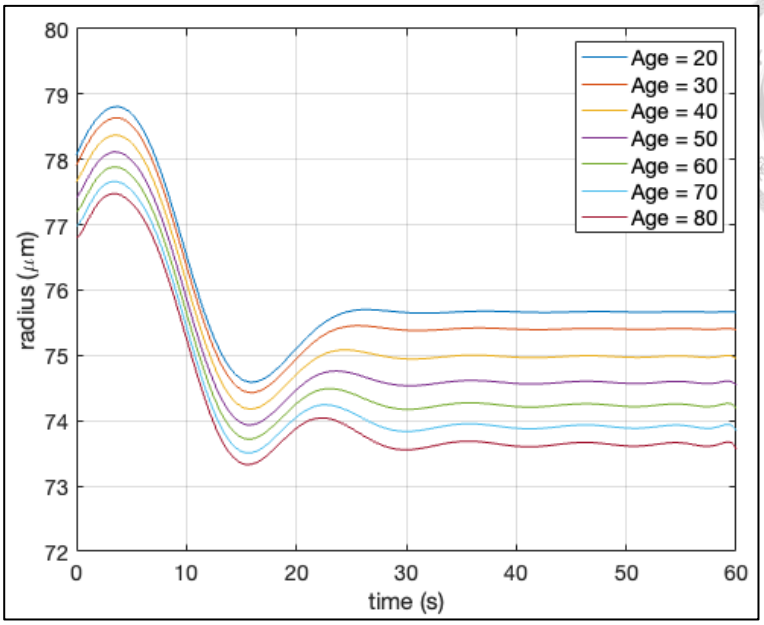

Figure 3.13 Dynamic radius for pressure rising from $P_a = 72\ mmHg$ to $80\ mmHg$ follow the different ages.

It is observed that due to ageing, vessel radius tends to decrease with age regardless of whether the pressure is increasing or decreasing, but the trend distribution across age groups remains broadly consistent. Therefore, we can further observe the trends in blood flow under dynamic conditions across different age groups as shown in Figures 3.14 and 3.15.

doi:10.6342/NTU202403077

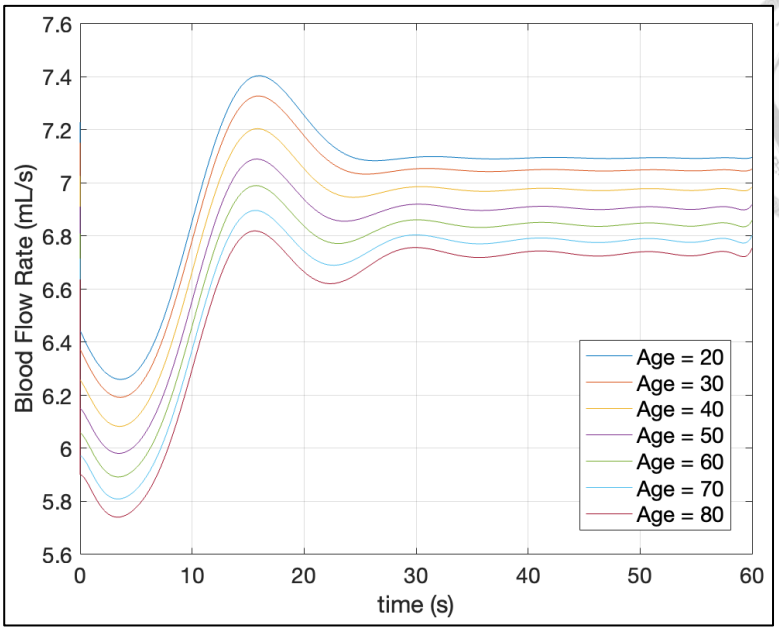

Figure 3.14 Dynamic flow rate for pressure drop from $P_a = 80\ mmHg$ to $72\ mmHg$ follow the different ages.

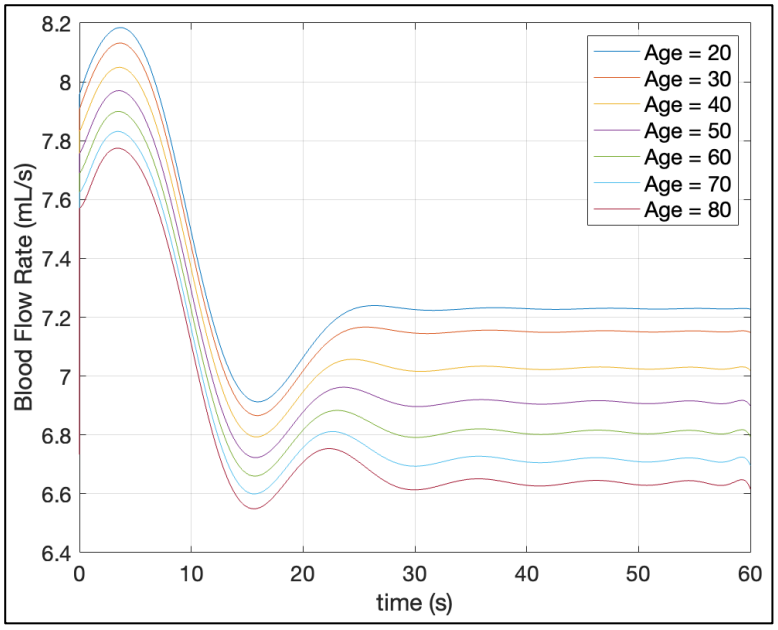

Figure 3.15 Dynamic flow rate for pressure rising from $P_a = 72\ mmHg$ to $80\ mmHg$ follow the different ages.

doi:10.6342/NTU202403077

The charts clearly demonstrate a decrease in blood flow as a result of ageing, indicating a progressive decline in vascular function with age. However, despite this overall decline, the pattern of how blood flow decreases[46] remains consistent across different age groups. This suggests that the physiological process of vascular ageing impacts individuals in a similar manner, progressively reducing the cerebral blood flow but maintaining a uniform pattern of decline. This consistency across age groups highlights the importance of regular monitoring and early intervention in managing age-related vascular changes.

doi:10.6342/NTU202403077

3.4 Conclusions

This chapter presents the results derived from the models and methods detailed in the previous chapter. Initially, the original model was used to establish a baseline curve for cerebral blood flow autoregulation, which served as a foundation for model fitting and set the initial condition for dynamic state analysis. Subsequently, parameters within the new mathematical model were adjusted, and the cerebral blood flow autoregulation curve was re-established. The study's findings further reveal that in dynamic states, blood flow maintains its symmetry in response to both increases and decreases in pressure. Additionally, the introduction of Tmax facilitated observations that the trend in blood flow across different age groups remains broadly consistent, which is crucial for understanding age-related vascular changes. To better integrate hypertension into this framework, future studies could focus on modifying autoregulation curves based on varying degrees of hypertensive conditions. This approach would allow for a more comprehensive analysis of how hypertension affects cerebral blood flow, thus enhancing the model's applicability in diagnosing and managing hypertension-related cerebral changes.

doi:10.6342/NTU202403077

Chapter 4

Conclusions and Future Work

The concluding chapter offers a comprehensive overview of the key findings from this thesis. It not only summarizes the primary results of our research but also briefly reviews the strengths and weaknesses of our methodology, along with exploring potential directions for future studies.

4.1 Summary of Findings

This thesis proposes the use of a new mathematical model to analyze the effects of ageing and hypertension on cerebral blood flow autoregulation. One of the main contributions of our work is the introduction of a novel model and numerical methods to re-establish the curve for cerebral blood flow autoregulation. This model not only simplifies the number of parameters and their complexity but also incorporates progressive vasoactive dysfunction to establish cerebral blood flow autoregulation curves that vary with age. These research focuses are introduced in Chapter Two.

In addition to the new mathematical model, Chapter Two also emphasizes the

doi:10.6342/NTU202403077

haemodynamic model. It employs Kirchhoff's laws in conjunction with the Hagen–Poiseuille equation to establish both the steady state and dynamic state of the whole-brain vascular model. Optimization utilizes various machine learning techniques such as gradient descent to fit all parameters within the new mathematical model. These analysis' findings provide light on the mechanisms underlying cerebral blood flow autoregulation.

Based on the outcomes of the optimisation and the new mathematical model, the following is a summary of the conclusions in this thesis:

1. Our proposed new mathematical model, which replaces the original model, can be applied to the analysis of cerebral blood flow autoregulation. It allows us to observe whether the response of cerebral blood flow autoregulation is altered and to determine if patients across different age groups are likely to experience ageing.

2. Compared to the original model has 44 parameters, the new mathematical model uses 11 parameters in Table 3.1, thus greatly reducing the computational resources needed for clinical data analysis.

doi:10.6342/NTU202403077

3. In the analysis of the dynamic state, it can be seen that the results established by the new mathematical model are broadly consistent with the literature[17]. Additionally, the introduction of progressive vasoactive dysfunction allows for the establishment of changes in vessel radius and blood flow across different age groups, which provides a good predictive tool for analysing the symptoms of ageing patients.

4.2 Limitations

Although the methods in this study show promise for replacing the existing model, there are notable limitations. For instance, we observed small discrepancies in the initial stages of the autoregulation curve. These discrepancies could be due to the model's sensitivity to initial parameter settings, which might not fully capture the dynamics of cerebral blood flow under lower blood pressure conditions. This leads to concerns about the model's applicability to patients with hypotension [40]. Initially, our study was tailored to better understand and predict cerebral blood flow autoregulation in patients with hypertension. However, with further refinement and calibration of the initial parameters, this model has the potential to be adapted for use in conditions of both high and low blood pressure, enhancing its versatility for broader clinical applications.

doi:10.6342/NTU202403077

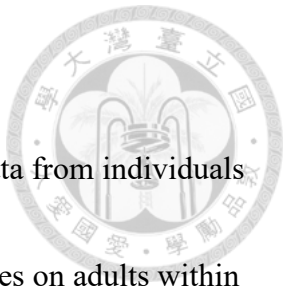

Secondly, our measurements and model development are based on data from individuals aged 20 and above, as is reflected in the literature that typically focuses on adults within this age group. Therefore, the model developed in this study is primarily applicable to adults and may not accurately represent the cerebrovascular dynamics of individuals under the age of 20, who may also suffer from cerebral blood flow disorders. This limitation necessitates continued reliance on traditional clinical diagnostic techniques for younger populations. Moreover, while we have extended the model's applicability up to 80 years old, this too is an approximation. Accurately modelling cerebral blood flow across the entire lifespan, from below 20 to over 80 years old, presents significant challenges due to the extensive physiological changes that occur with ageing.

Another limitation arises from the mathematical assumptions made in Section 2.2.2 to reduce the model's complexity. These assumptions include that blood flow changes slowly enough over time, vessel walls do not alter under stress, loads are distributed axially symmetric along the vessel, and strain on the vessel cross-section is uniform across all sections. Although our results closely align with real-world scenarios as per existing studies, the model still offers scope for further refinement. Future work could

doi:10.6342/NTU202403077

focus on optimizing the model to achieve a closer fit with more detailed experimental data across all ages, thereby enhancing its utility in clinical diagnostics and broadening its applicability.

4.3 Future Work

Although the new mathematical model proposed in this study marks a significant advancement towards improved analysis of cerebral blood flow autoregulation, it necessitates further validation and new research directions in the future. While this study introduces a new mathematical model aimed for clinical application, its practical use will require rigorous validation with clinical patient data, akin to the procedures undertaken to validate the original model in earlier research [36]. Future work will need to focus on this validation process, which could involve comparing the predictions of the new model against a wide range of clinical outcomes and established benchmarks in diverse patient groups. It may also include longitudinal studies to track the model's predictive accuracy over time or under different physiological conditions. Completing these steps will be essential to demonstrate conclusively that the new mathematical model can fully substitute the original model and provide reliable, actionable insights in

doi:10.6342/NTU202403077

clinical settings.

Furthermore, as well as proceeding with the full clinical validation of the new mathematical model, it will also be introduced into the realm of fitness and exercise. This initial application is supported by research indicating that progressive physical training does not significantly alter autoregulation capabilities [41]. Moreover, studies have found no notable differences in cerebral blood flow autoregulation between young healthy individuals who engage in prolonged sitting and exercise [42], and elderly individuals who have maintained a lifelong habit of exercise [43]. To implement the new model in fitness and exercise, it would be possible to conduct controlled studies that measure cerebral blood flow responses during different types of physical activities and training regimes. By analyzing these responses, the model's utility in predicting changes in cerebral autoregulation due to exercise can be assessed. This approach will provide valuable insights into how regular physical activity influences cerebral blood flow dynamics, thereby enhancing our understanding of the interplay between fitness, exercise, and brain health. This preliminary application will also help refine the model by exposing it to real-world scenarios before it is employed in more complex clinical settings.

doi:10.6342/NTU202403077

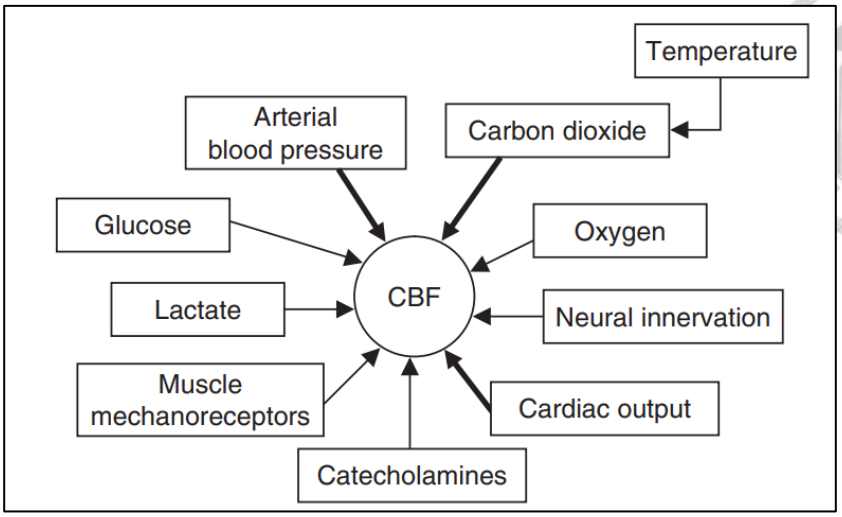

Figure 4.1 Regulating factors of cerebral blood flow (CBF) during exercise. (Figure reproduced from [48]).

A key objective is to use the new mathematical model to analyse the effects of ageing and hypertension on cerebral blood flow autoregulation. If future validation of the model is successful, it is anticipated that it will entirely replace the original computational model, thereby supporting research and significantly reducing computational resource requirements. Continued progress in computational modelling, data validation methods, and interdisciplinary collaboration are crucial to fully realising the potential of these efforts.

doi:10.6342/NTU202403077

References

[1] PAYNE, Stephen J. *Cerebral Autoregulation：Control of Blood Flow in the Brain*. 2016.

[2] RAHMA, Ahmed G., et al. Blood flow CFD simulation on a cerebral artery of a stroke patient. *SN Applied Sciences*, 2022, 4: 261.

[3] GROEN, D., et al. Validation of Patient-Specific Cerebral Blood Flow Simulation Using Transcranial Doppler Measurements. *Computational Physiology and Medicine*, 2018, 9: 721.

[4] https://open.oregonstate.education/aandp/chapter/18-1-functions-of-blood/

[5] CASSON, N. A Flow Equation for Pigment-Oil Suspensions of the Printing Ink Type. *Oxford*, 1959, 84-104.

[6] CLAASSEN, AHR J. Transfer function analysis of dynamic cerebral autoregulation-A white paper from the International Cerebral Autoregulation Research Network. *CARNet*, 2016, 36.4: 665-680.

[7] LEUNG, J., et al. Developmental trajectories of cerebrovascular reactivity in healthy children and young adults assessed with magnetic resonance imaging. *Neuroscience*, 2016, 594.10: 2681-2689.

doi:10.6342/NTU202403077

[8] GRAFF, Barnaby J., et al. Regional Cerebral Blood Flow Changes in Healthy Ageing and Alzheimer's Disease: A Narrative Review. *Cerebrovascular Disease*, 2023; 52:11-20.

[9] https://www.ndc.gov.tw/Content_List.aspx?n=0F11EF2482E76C53

[10] WHITWORTH, Judith A. 2003 World Health Organization (WHO) :International Society of Hypertension (ISH) statement on management of hypertension. *J Hypertension*, 2003, 21.11:1983-92.

[11] https://www.hpa.gov.tw/Home/Index.aspx

[12] FARACO, G., et al. Hypertension: a harbinger of stroke and dementia. 2013, 62.5:810-7.

[13] https://medicine.utah.edu/radiology/research/learn/pet

[14] https://my.clevelandclinic.org/health/diagnostics/4876-magnetic-resonance-imaging-mri

[15] MILLER, Kathleen B., et al. Age-Related Reductions in Cerebrovascular Reactivity Using 4D Flow MRI. *Original Research*, 2019, 11.10.

[16] TONG, Z., et al. A multiscale model of cerebral autoregulation. *Medical Engineering and Physics*. 2021, 95:51-63.

doi:10.6342/NTU202403077

[17] CATHERALL, M. Modelling the role of nitric oxide in cerebral autoregulation. *Oxford University Press*; 2014.

[18] BAYLISS, WM. On the local reactions of the arterial wall to changes of internal pressure. *J Physiol*, 1902; 3.28: 220–31.

[19] HAI, CM, et al. Cross-bridge phosphorylation and regulation of latch state in smooth muscle. *Am J Physiol*, 1988; 1.254: C99–106.

[20] YANG, J, et al. The myogenic response in isolated rat cerebrovascular arteries: smooth muscle cell model. *Med Eng Phys*, 2003; 8.25: 691–709.

[21] STÅLHAND, J, et al. Smooth muscle contraction: Mechanochemical formulation for homogeneous finite strains. *Prog Biophys Mol Biol*, 2008; 1.96: 465–81.

[22] GALANTAI, A. The theory of Newton's method. *Journal of Computational and Applied Mathematics*, 2000, 124: 25-44.

[23] SMITH, DR. *An Introduction to Continuum Mechanics - after Truesdell and Noll*. 1993.

[24] BAEK, S, et al. Biochemomechanics of Cerebral Vasospasm and its Resolution: II. Constitutive Relations and Model Simulations. *Annals of Biomedical Engineering*, 2007, 9.35: 1498-1509.

doi:10.6342/NTU202403077

[25] VALENTÍN, A, et al. A Multi-Layered Computational Model of Coupled Elastin Degradation, Vasoactive Dysfunction, and Collagenous Stiffening in Aortic Aging. *Annals of Biomedical Engineering*, 2011, 7.39: 2027-2045.

[26] FELDMAN, SA, et al. Transmedial collagen and elastin gradients in human aortas: reversal with age. *Atherosclerosis*, 1971, 3.13: 385–394.

[27] CARDAMONE, L, et al. Modelling carotid artery adaptations to dynamic alterations in pressure and flow over the cardiac cycle. *Math. Med. Biol*, 2010, 4.27: 343–371.

[28] VALENTÍN, A, et al. Parameter sensitivity study of a constrained mixture model of arterial growth and remodeling. *J. Biomech. Eng*, 2009, 10.131: 10100.

[29] HUMPHREY, JD. Cardiovascular Solid Mechanics: Cells, Tissues, and Organs. *New York: Springer*, 2002.

[30] ARRIBAS, SM, et al. Elastic fibres and vascular structure in hypertension. *Pharmacol. Ther*, 2006, 3.111: 771–791.

[31] MATLAB, Starting. Matlab. *The MathWorks, Natick, MA*, 2012.

[32] https://www.mathworks.com/help/matlab/ref/fzero.html

[33] RUDER, S. An overview of gradient descent optimization algorithms. *arXiv*, 2017.

doi:10.6342/NTU202403077

[34] https://www.mathworks.com/help/matlab/ref/ode45.html

[35] CHAPRA, S. *Applied Numerical Methods with MATLAB: for Engineers & Scientists*, 2004.

[36] KUO, L, et al. Interaction of pressure- and flow-induced responses in porcine coronary resistance vessels. *Am J Physiol*, 1991, 6.261: H1706–15.

[37] URSINO, M, et al. Theoretical analysis of complex oscillations in multibranched microvascular networks. *Microvasc Res*, 1996, 2.51: 229-49.

[38] https://www.mathworks.com/help/optim/ug/fmincon.html

[39] PAYNE, Stephen J. *Cerebral blood flow and metabolism: a quantitative approach*. 2018.

[40] OGOH, S, et al. Influence of baroreflex-mediated tachycardia on the regulation of dynamic cerebral perfusion during acute hypotension in humans. *J Physiol*, 2010, 15.588: 365-71.

[41] DESOUZA, CA, et al. Regular aerobic exercise prevents and restores age-related declines in endothelium-dependent vasodilation in healthy men. *Circulation*, 2000, 12.102: 1351-7.

[42] GUINEY, H, et al. Evidence cerebral blood-flow regulation mediates exercise-cognition links in healthy young adults. *Neuropsychology*, 2015, 1.29: 1-9.

doi:10.6342/NTU202403077

[43] COLCOMBE, SJ, et al. Aerobic exercise training increases brain volume in aging humans. *J Gerontol A Biol Sci Med Sci*, 2006, 11.61: 1166-70.

[44] https://www.fda.gov/radiation-emitting-products/medical-x-ray-imaging/computed-tomography-ct

[45] ANTONELLO, D, et al. Transcranial Doppler Ultrasound: Physical Principles and Principal Applications in Neurocritical Care Unit. *J Cardiovasc Echogr*, 2016, 2.26: 28-41.

[46] HANZHANG, L, et al. Alterations in Cerebral Metabolic Rate and Blood Supply across the Adult Lifespan. *Cerebral Cortex*, 2011, 6.21: 1426-34.

[47] IRGENS, F. *Tensor Analysis*. 2019.

[48] QUERIDO, JS, et al. Regulation of Cerebral Blood Flow During Exercise. *Sports Medicine*, 2007, 9.37: 765-782.

doi:10.6342/NTU202403077